ORIGINAL ARTICLE

Identifying controlling factors for the evolution of shallow groundwater chemistry of Ellala catchment, northern Ethiopia

Grmay Kassa Brhane[1] · **Hailemariam Siyum Mekonen**[1]

Abstract

This study was designed to deal with the identification of the hydrogeochemical and anthropogenic processes controlling the evaluation of groundwater chemistry in the Ellala catchment covering about 296.5 km^2 areal extent. The chemical analysis revealed that the major ions in the groundwater are Ca^{2+}, Mg^{2+}, Na^+, and K^+ (cations) and HCO_3^-, PO_4^{3-}, Cl^-, NO_3^- and SO_4^{2-} (anions), and most of the groundwater samples (68.42%), revealed that the groundwater in the catchment is non-alkaline in nature, and the solid materials and liquid wastes discharged from different sources could be the main sources for pH and EC in the groundwater in addition to the aquifer material contribution. It is observed that the EC of the groundwater is fairly correlated with the DTS which indicates that highly mineralized water is more conductor than water with low concentration. The degree of salinity of the groundwater is increased along the groundwater flow path from east to west and is high surrounding Mekelle City due to the liquid and solid wastes discharged from the city and the industries. The groundwater facies in the catchment predominated with calcium, magnesium, and bicarbonate and the groundwater type is mainly Ca–Mg–HCO3 and Mg–Ca–HCO3. The main geochemical processes controlling the evolution of the groundwater chemistry in the catchment are rock–water interaction, particularly carbonate dissolution and reverse ion exchange due to the clay layer in the aquifer. Non-significant silicate weathering and halite dissolution also contributed to the evolution of groundwater chemistry in the catchment. The groundwater in the catchment is dominated by the meteoritic origin although it needs further groundwater chemistry study with isotope dating analysis. The groundwater is in an undersaturated state with the calcite, dolomite, and aragonite minerals where the further dissolution of these minerals is going in the groundwater. The main source of calcium and magnesium in groundwater is the dissolution of carbonate minerals (calcite and dolomite) since carbonate rocks are the dominant aquifer materials in the catchment. In addition to this, the weathering of dolerite rock is also a possible source of magnesium ions. The relatively higher concentration of sodium over chloride indicates the source for sodium ion is reverse ion exchange and/or weathering of sodium-bearing materials (such as shale and dolerite) rather than halite dissolution. The high concentration of phosphate, nitrate, and chloride in the groundwater is the main anthropogenic source that needs treatment and groundwater quality control and management in the catchment. From the Base Exchange index analysis, it is noticed that the groundwater in the catchment is dominated by the meteoritic origin, although it needs further groundwater chemistry study with isotope dating analysis.

Keywords Ellala catchment · Factor · Chemistry · Geochemical · Groundwater

Introduction

Groundwater is subsurface water that occurs in soils and rocks beneath the water table (Aminiyan et al. 2016). Groundwater plays a significant role in the development of a nation. All over the world, groundwater is widely used for different purposes such as domestic, irrigation, industry, and recreational. The use of groundwater has increased rapidly in the recent few years due to rapid population growth, drought,

✉ Grmay Kassa Brhane
grmay.kassa@adu.edu.et

Hailemariam Siyum Mekonen
hsiyum2007@yahoo.com

1 Department of Geology, Adigrat University, Adigrat, Ethiopia

and rapid growth of the world economy (Aminiyan et al. 2020; Ostad-Ali-Askari et al 2021).

The chemistry of groundwater is derived from the interaction between groundwater and subsurface earth materials, the chemistry of rainwater, and various anthropogenic sources, such as mining, land clearance, saline intrusion, and industrial and domestic wastes (Babiker et al. 2007; Llamas and Martínez-Santos 2005; Talebmorad et al. 2022). The most important hydrogeochemical processes that control the composition of groundwater are the dissolution of minerals from the aquifer materials, precipitation of minerals from groundwater, and ion exchange processes between the aquifer materials and groundwater. Analysis of groundwater chemistry is vital to understanding the influence of geology, climate, and anthropogenic activities on groundwater composition, and it is important to evaluate the suitability of water for different uses, such as drinking, agriculture, and industries (Bucci et al. 2017; Shayannejad et al. 2022). The principal factors that have significant effects on the evolution of the chemical composition of groundwater can be identified from the relationships of major ions (Ahmed & Clark 2016; Fisher and Mullican 1997; Ostad-Ali-Askari et al. 2019).

So far, various hydrogeochemical works have been conducted to understand the geochemical processes that are affecting groundwater chemistry and quality (Tirumalesh et al 2010; Rajesh et al 2012; Moussaoui et al 2023; Argamasilla et al 2017; Choi et al 2014; Dehbandi et al 2018; Liu et al 2017; Rao et al. 2012). Sufficient knowledge of the geochemical processes that govern the evolution of groundwater chemistry important to groundwater-related issues, and the hydrogeochemical processes are significantly variable based on time and space (SubRamani et al. 2010).

Currently, the main source of water supply for domestic purposes is groundwater in most parts of Ethiopia both in urban and rural areas. Besides this, groundwater is also extensively used for irrigation purposes in the Tigray region due to the scarcity of surface water and insufficient rainfall in most parts of the region. The Ellala and Aynalem wellfields are the main sources of groundwater for water supply in Mekelle City and surrounding areas. The regional hydrogeological setting of the whole or large part of the Mekelle basin was studied by various researchers (Abreha 2014; Grmay et al. 2015).

Understanding the roles of hydro-geochemical processes in the evolution of groundwater chemistry in developing countries like Ethiopia is limited, rather most of the studies were focused on the assessment and evaluation of groundwater quality for different uses. As the catchment is close to Mekelle City which is fast-growing than ever, the water supply for different purposes such as domestic, industrial, and irrigation is mined from groundwater. So far the groundwater assessment and some unintegrated works on groundwater

chemistry have been routine previous works as mentioned above. However, for a better understanding of the hydrogeochemical processes which have been undergone in the groundwater, comprehensive and integrated analysis with multiple binary cations and anion analysis is vital due to the heterogeneity of the aquifer system (Grmay et al 2015), and active industrial practice in the catchment. Moreover, the knowledge of the scientific justification of the hydrogeochemical dynamism as a factor affecting the gradual evolution of groundwater chemistry is limited. Consequently, people and scholars who have a routine idea about groundwater quality, have doubts about the sources of groundwater chemistry and geochemical processes that control the evolution of groundwater chemistry in different areas. Therefore, this study focuses on the hydrogeochemical factors with comprehensive and integrated multi-binary cation and/or anion analysis. Furthermore, particular attention has been given how their impact on the evolution of groundwater chemistry, thereby adding input to the knowledge and understanding of the area of hydrogeochemical process between groundwater and aquifer interaction in various aquifer systems.

Description of the study area

Location

The Ellala catchment is located in the central part of the Mekelle Basin and west of the Afar Rift Valley. It is found in northern Ethiopia in Tigray regional, state, and bounded between 1475000 m–1515000 m N and 520000 m–580000 m E (Fig. 1A). The study area covers about 296.5 km2.

Physiography and climate

The catchment is characterized by cliffs at the northern and southern peripheries of the catchment, ridges in the eastern, northeastern, and southeastern parts, and a flat area in the western part of the catchment (Fig. 1B). The maximum elevation is 2620 m asl in the eastern part of the catchment, whereas the minimum elevation is 1960 m asl in the western part of the catchment.

This catchment is part of the Tekeze drainage system. In this catchment, there is one main river which is known as the Ellala River and many tributaries. This main river follows the structurally weak plane of the Mekelle fault which intersects different lithological units, whereas the tributaries follow the general slope inclination (Abreha 2014; Grmay et al 2015). The low density of streams may indicate that the bedrock is either highly resistant or highly permeable. The highly resistant bedrock may be related to dolerite dykes, whereas the permeable nature is associated with highly
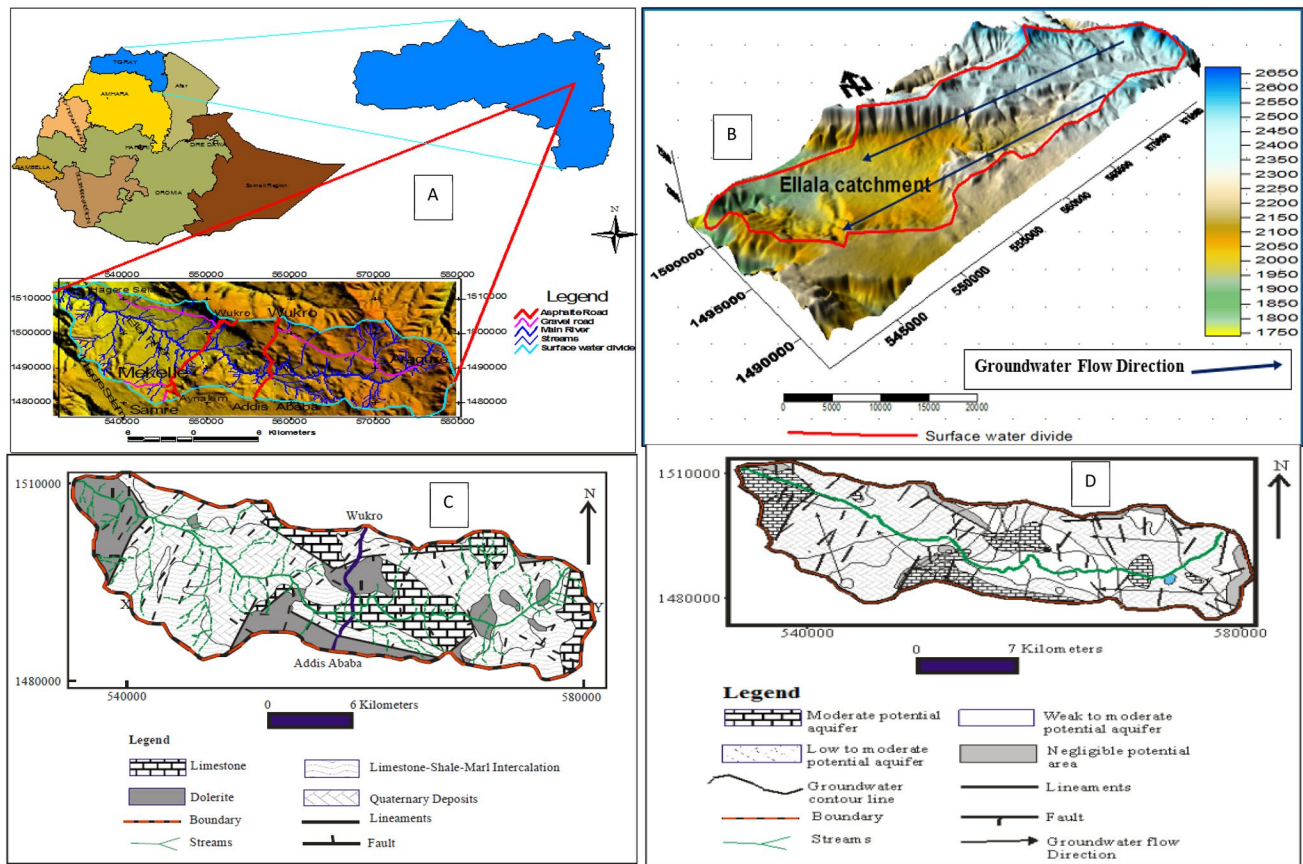
Fig. 1 **A** Location and drainage map **B** 3D physiographic view **C** Geological Map **D** Hydrogeological map Basin (Kassa et al., 2015)

fractured and jointed bedrock. It is characterized by a dendritic drainage pattern (Fig. 1A).

The climate of Ethiopia is mainly controlled by the seasonal migration of the Intertropical Convergence Zone (ITCZ) and the topographical features of the area (Fazzini et al. 2015). According to Ethiopian temperature zoning, the catchment is located under the semi-arid climatic zone. There are two rainy seasons, June to September and March to April. However, most of the annual rainfall occurs during July and August with a mean annual rainfall of 650 mm. The mean annual temperature ranges from 15 to 16 ℃.

Geological setting

Regional geology and geological structures

The Ellala basin lies almost at the center of the Mekelle Basin. Scholars (Beyth, 1972b; Kazmin, 1972), have studied the regional geology of the Mekelle Basin. Accordingly, the Mekelle Basin is one of the five well-known sedimentary basins in Ethiopia, which is composed of very thick Palaeozoic—Mesozoic sedimentary rocks. The Palaeozoic sediments rest on the folded and eroded surface of the Precambrian basement and are unconformably overlain by the Mesozoic sediments (Beyth, 1972b; Kazmin, 1972). The Mesozoic sediments unconformably are overlain by flood basalts of the Tertiary age (). The Mesozoic sediments from the oldest to the oldest are the Adigrat sandstone, Antalo limestone, the Agula shale, and Amba Aradom sandstone. These sediments are the results of major transgression–regression cycles and are related to major regional tectonic events that have affected the entire East African region (Ayele and Gangadharan 2016). In the basin, there are regional brittle and ductile structures. The Negash Geosynclinal Fold is the Neoproterozoic structure in Mekelle Outlier and is an overturned fold plunging southward by about 15 to 20^0 (Gebreyohannes 2009). The four regional normal fault belts in the Mekelle Basin are the Wukro, Mekele, Chelekwot, and Fuicea Mariam fault belts (Beyth 1972a). These faults were probably active after the deposition of the Agula Shale but before the deposition of the Amba Aradam Formation.

Local geology and geological structures

The major geological units in the Ellala catchment are limestone, limestone–shale–marl intercalation, dolerite intrusion, and Quaternary sediments (Fig. 1C; (Grmay et al 2015).

Generally, the limestone and limestone–shale–marl intercalation beds are horizontal but tilted near the dolerite intrusion and in fault zones and the dip angle of the beds varies from 10° to 25°. These rock units are affected by minor and major faults and joints. These joints are both systematic and non-systemic and regular joint spacing and an aperture range from 0.4 to 2 m and from 0.6 to 10 cm, respectively. Besides, karstic features are common in limestone. Dolerite dykes and sills have intruded on these units in different places. The dolerite unit covers a large area and is affected by joints. However, the joints are widely spaced and have very narrow apertures as compared with other rock units. It is hard and massive, but in some places, it is highly weathered and an exfoliation type of weathering is common in this rock unit. The dolerite intrusions follow the fault zone of the main Mekelle fault belt. The quaternary sediments are composed of boulders, gravel, sand, silt, and clay-sized particles. These sediments are mainly found in flat topography and along the main Ellala River and their thickness varies from 0.8 to 5 m.

The major geological structure in the catchment is a fault, and the Mekelle fault belt is found in this catchment with an orientation of NW–SE and dipping southward. The orientations of regional and local faults are grouped into two NW–SE and NE–SW. Faults with an NW–SE orientation are mainly found in the vicinity of Mekelle City, whereas faults trending in the NW–SE are found widely distributed throughout the catchment (Fig. 1C; Beyth 1972a).

Hydrogeology of Ellala catchment

The hydrogeology setting of the catchment is very complex because the sedimentary rocks are intruded by complex networks of dolerite dykes and sills. The rock units in the catchment are highly affected by regional and local structures (faults and joints). Moreover, solution cavities and caverns are common in the limestone unit. Hence, these features have a primary role in the occurrence and movements of groundwater in the catchment. The main aquifer units of the Ellala catchment are highly weathered and fractured limestone and shale–limestone intercalated, dolerite, and shale units (Fig. 2; (Grmay et al 2015)). These units show a wide range of hydraulic properties and the highest hydraulic conductivity values were recorded at the contacts between the sedimentary rocks and dolerite intrusion due to a high degree of fracturing and weathering at the contact zones (Yehdego 2003). The types of aquifers in the catchment are mainly unconfined and confined to semi-confined (Fig. 2)

and the aquifer productivity in the catchment ranges-from poor to moderate potential (Fig. 1D; (Grmay et al 2015)).

A groundwater level contour map was prepared using the groundwater level of 49 wells, and the groundwater, flows from east to west, is the same as the surface water flow direction (Grmay et al 2015). The groundwater flow path can be inferred from the ratio of bicarbonate to chloride (Signal, 1999). Decreasing the ratio of bicarbonate to chloride concentration from the east toward the western part of the catchment supports the idea that groundwater flows from east to west (Fig. 1D). The Ellala River is parallel to the fault plane of the Mekelle fault. Therefore, the groundwater movement or flow path in the catchment is mainly controlled by the major and minor structures.

Materials and methods

Water sample collection

The depth-integrated groundwater sampling method has been applied because the groundwater sampling was conducted after the wells' drilling processes were completed. Collection of groundwater samples from all wells and springs in the catchment is time-consuming and it is not economically viable to conduct chemical analysis for all samples. Hence, before sample collection, in situ measurements of electrical conductivity, pH, temperature, and TDS were conducted on 105 groundwater points with portable EC and pH meter devices during the field investigation. Once the groundwater samples have been stratified, the selection of representative samples for analysis from each stratification or class is the precondition for laboratory analysis of the groundwater samples. Both groundwater sample stratification and selection have been done based on the Quality classification of water for irrigation (after Wilcox 1955). Accordingly, 38 representative groundwater samples were selected by applying a random sampling technique from each class by considering the distribution of wells in the catchment and the different lithological units. As a result, twenty-two samples from shallow wells, nine samples of hand-dug wells, and seven samples from springs were selected. After the groundwater sample selection for analysis had been done, two samples per each selected groundwater point were collected using one litter capacity of plastic bottles. From these water points, two deep wells, two springs, eight shallow wells, three hand-dug wells, and one open well are in quaternary deposits, two springs, three shallow wells, and one hand-dug well and two open wells are in dolerite, one spring is in limestone and one deep well, nine shallow wells, two springs, and one open well are in limestone–shale–marl interaction.
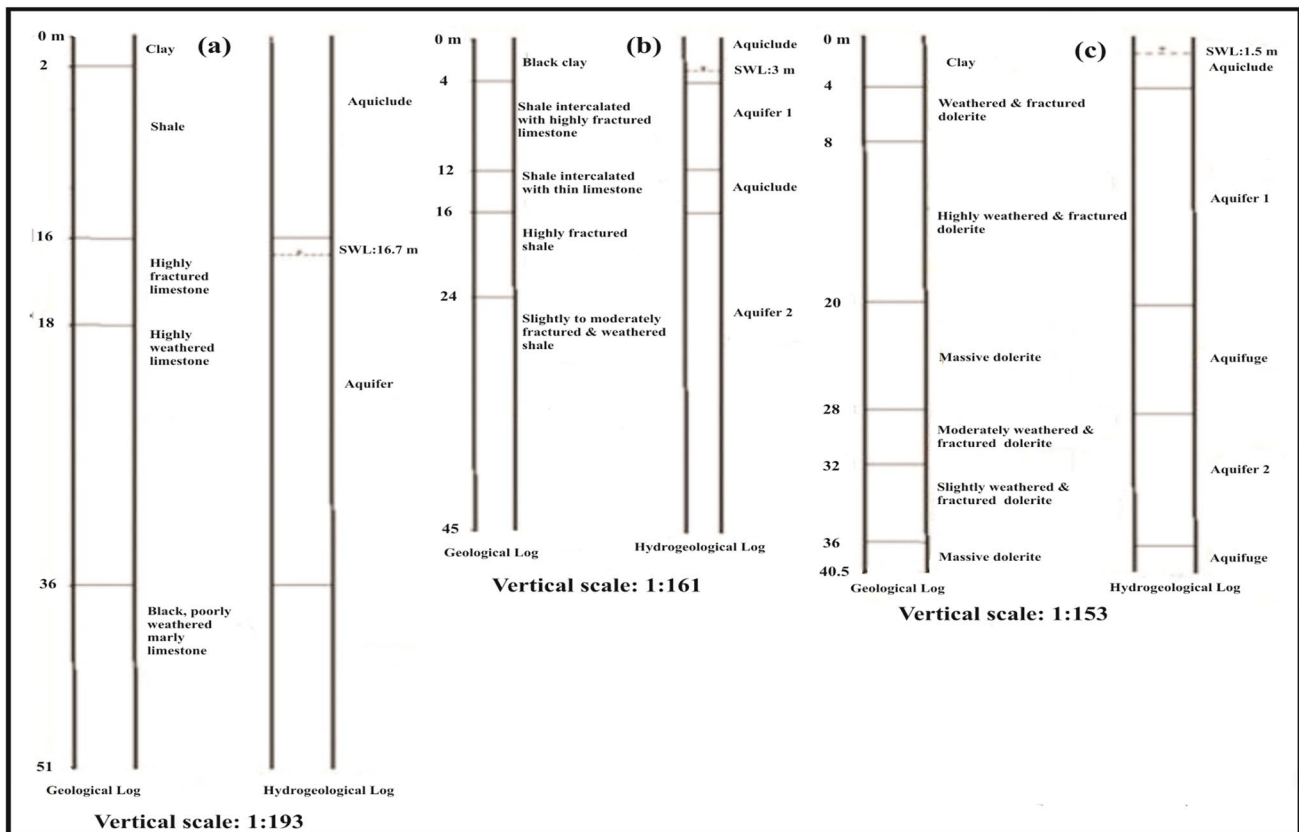
Fig. 2 Lithological and hydrogeological Log **a** Limestone Aquifer **b** Limestone-Shale-Marl Intercalation Aquifer **c** Dolerite Aquifer. (Modified after Grmay et al 2015)

In situ measurements physical parameters

The most valuable physical parameters of groundwater, such as temperature, pH, TDS, and electrical conductivity, were made in the field.

Laboratory analysis

The groundwater samples were analyzed for their chemical concentration in the hydrogeochemistry laboratory of Earth Sciences at Mekelle University.

Laboratory analysis for all samples was done for their major cations and anions (Na^+, Ca^{2+}, Mg^{2+}, K^+, Cl^-, SO_4^{2-}, HCO_3^-, NO_3^{1-}, and PO_4^{3-}. To analyze the cations (Na^+, Ca^{2+}, Mg^{2+}, and K^+) of the samples, an atomic absorption spectrometer was used and a titrimetric method in the lab was used to analyze HCO_3^- and Cl^-. Moreover, anions, such as SO_4^{2-}, NO_3^{2-}, and PO_3^{2-}, of the samples were measured using an Ultra Spectrophotometer. (Tables 1, 2, 3, 4).

Personal and instrumental errors

Since the chemical analysis was done based on the predefined objective of the work, it was clear that there some chemical concentrations that had been remained from the analysis. As a result, it was planned to use duplication analysis rather than ionic error balance. Hence, the sample analysis was conducted two times where the analysis was run twice, and the chemical analysis of these samples showed a good repetition with very small variations (Table 5 & 6).

Hydrochemical data analysis

Schoeller and piper diagram analysis To determine the dominant ions in the groundwater and hence the groundwater facies, both the cations and anions of the groundwater samples were plotted on the Schoeller diagram (Schoeller 1955) and Piper diagram (Piper 1944), using AquaChem 3.7 software. From these analyses, it is possible to identify the various groundwater facies and water types. In addition to this, the Schoeller diagram (Schoeller 1955) was done to

Table 1 Physical- chemical parameters of groundwater samples of the Ellala catchment (concentration of ions in mg/l, temperature (T) in ^{0}C and EC in µS/cm)

Sample code	pH	EC	T	Ca^{2+}	Mg^{2+}	Na^+	K^+	HCO_3^-	Cl^-	SO_4^{2-}	NO_3^-	PO_4^{3-}	TDS
SP1	6.3	1039	19.2	72	42	14	88	353.8	4.2	3.2	1.0	45.7	623.9
SP6	6.2	1369	17.5	153	78	22	43	311.1	4.9	2.3	0.4	30.4	645.2
OPW2	6.3	1685	19.2	90	60	19	68	457.5	4.6	3.7	0.5	4.0	707.2
SHW18	7.1	2030	23.3	140	98	16	61	347.7	6.8	3.3	1.0	22.1	696.0
SHW19	7.6	640	21.8	192	102	14	62	329.4	19.6	16.9	0.7	17.1	753.8
DPW16	8.1	970	25.6	178	120	106	70	268.4	30.6	22.3	0.4	27.2	822.9
SHW8	6.4	730	17.5	216	160	12	99	359.9	20.8	4.0	7.3	29.5	908.5
SHW26	7.3	1130	24.5	173	116	25	50	390.4	10.9	6.2	1.6	30.7	803.7
SHW31	5.9	1790	22.8	168	109	45	92	457.5	10.5	65.0	0.2	20.1	967.3
DPW20	7.1	1240	25	146	99	61	27	378.2	17.8	85.5	8.1	94.3	916.9
HDW2	6.3	1202	18.2	135	68	14	66	402.6	6.4	3.6	9.6	22.1	727.3
SP18	6.6	910	20	165	98	55	46	366	15.4	5.4	7.8	23.0	781.6
HDW13	7.6	760	24.8	178	120	8	92	384.3	13.4	4.0	8.7	25.3	833.7
SHW32	6.4	640	22.5	146	113	15	46	408.7	7.1	5.1	7.6	23.6	772.1
SHW36	6.0	1031	19.1	205	34	15	102	433.1	4.8	3.8	2.7	15.1	815.5
SP23	6.4	778	19.8	45	48	15	43	347.7	3.9	3.2	10.7	17.0	533.5
SP24	6.0	1243	21.4	72	32	18	45	402.6	3.8	2.9	1.1	22.8	600.1
SHW37	6.2	1037	21.9	50	24	12	40	329.4	1.6	3.7	0.8	94.6	556.0
SHW38	6.3	1133	21.2	53	78	36	80	542.9	1.6	5.5	6.8	20.9	824.6
HDW18	6.2	1180	21.8	64	48	16	62	372.1	1.9	3.1	1.2	22.1	590.4
SP12	7.0	320	23.1	90	72	12	77	396.5	3.7	5.1	1.6	51.3	709.3
SHW6	5.8	980	20.8	164	120	19	67	390.4	11.7	3.1	7.1	28.5	810.8
SHW7	5.7	520	21.4	206	106	20	35	353.8	19.6	4.8	2.2	20.3	767.7
OPW3	6.6	1280	20.2	153	98	23	52	280.6	12.4	4.8	7.4	39.1	670.3
SHW21	8.1	640	23.1	196	34	37	50	701.5	18.7	5.3	1.0	24.0	1067.4
OPW1	6.4	574	19	123	87	3	59	329.4	4.9	3.9	4.8	28.1	643.1
SHW25	6.9	630	22	186	98	5	36	481.9	13.9	4.0	1.3	18.0	844.1
SHW35	6.4	527	18.5	67	66	7	47	244	3.8	4.5	8.7	22.6	470.6
SHW39	6.3	643	21.3	64	68	39	42	298.9	2.6	2.5	1.2	2.5	520.7
SHW43	7.6	2520	25.3	120	89	20	29	308.66	14.5	5.6	2.5	20.7	609.9
OPW8	6.9	1970	23.9	163	98	13	47	384.3	8.6	10.0	0.7	22.2	746.8
OPW7	6.5	2060	23	154	87	62	77	347.7	12.9	6.8	0.3	24.7	772.4
HDW10	8.1	2370	24.4	176	87	22	56	536.8	16.7	7.6	7.1	24.3	933.5
SHW3	6.0	2180	19.8	125	65	20	29	402.6	4.4	5.5	6.8	34.0	692.2
SHW48	7.3	3012	25.6	98	56	13	47	396.5	9.2	23.9	9.1	28.8	681.5
SP20	6.7	50	24.3	166	68	62	77	285.48	5.1	4.8	4.4	32.2	705.0
SHW40	7.4	3121	25.8	88	22	53	0	433.1	23.4	5.8	6.8	94.0	726.2
DPW19	6.8	3050	23.8	76	8	56	0	384.3	24.2	65.2	9.5	92	548.5

identify the dominant cations and anions which can provide clues on the respective sources of these components.

Multi-variant binary analysis

Different binary plot analyses were done to identify the predominant hydrogeochemical processes that govern the groundwater chemistry in the catchment (Abid et al. 2011; Kloppmann et al. 2011). Hence, analysis of the binary plots and ratios between commonly bonded cations and anions was performed to identify the geochemical

and anthropogenic factors that control the evolution of the groundwater chemistry in the catchment.

a) The degree of rock-water interaction and its impact on the evolution of groundwater chemistry were examined by the binary plots of TDS versus Na/ (Na + Ca) and TDS versus Cl/ (Cl + HCO3) (Gibbs 1970).

b) The binary plot analysis of Ca/Na versus HCO3/Na and Ca/Na versus Mg/Na was performed to determine the rock-water interaction domain which includes dissolution such as carbonate dissolution, evaporate dissolution,

Table 2 Groundwater type of the Ellala catchment

Sample code	Water type	Sample code	Water type
DPW16	Mg–Ca–Na–HCO3	SHW32	Mg–Ca–HCO3
DPW19	Ca–Na–HCO3	SHW35	Mg–Ca–HCO3
DPW20	Mg–Ca–HCO3	SHW36	Ca–Mg–K-HCO3
HDW10	Ca–Mg–HCO3	SHW37	Ca–Mg–HCO3
HDW13	Mg–Ca–HCO3	SHW38	Mg–Ca–HCO3
HDW18	Mg–Ca–K–HCO3	SHW39	Mg–Ca–Na–HCO3
HDW2	Ca–Mg–HCO3	SHW40	Ca–Na–Mg–HCO3
OPW1	Mg–Ca–HCO3	SHW43	Mg–Ca–HCO3
OPW2	Mg–Ca–HCO3	SHW48	Ca–Mg–HCO3
OPW3	Mg–Ca–HCO3	SHW6	Mg–Ca–HCO3
OPW7	Ca–Mg–Na–HCO3	SHW7	Ca–Mg–HCO3
OPW8	Ca–Mg–HCO3	SHW8	Mg–Ca–HCO3
SHW18	Mg–Ca–HCO3	SP1	Ca–Mg–K–HCO3
SHW19	Ca–Mg–HCO3	SP12	Mg–Ca–K–HCO3
SHW21	Ca–Mg–HCO3	SP18	Ca–Mg–HCO3
SHW25	Ca–Mg–HCO3	SP20	Ca–Mg–Na–HCO3
SHW26	Mg–Ca–HCO3	SP23	Mg–Ca–HCO3
SHW3	Ca–Mg–HCO3	SP24	Ca–Mg–HCO3
SHW31	Mg–Ca–HCO3	SP6	Ca–Mg–HCO3

Table 3 Chloro-alkaline Indices I and II

Sample Code	CAI-I	CAI-II	Sample Code	CAI-I	CAI-II
SP$_1$	− 23.14	− 0.47	HDW$_{18}$	− 41.58	− 0.36
SP$_6$	− 13.88	− 0.37	SP$_{12}$	− 22.87	− 0.36
OPW2	− 18.78	− 0.32	SHW$_6$	− 6.70	− 0.34
SHW$_{18}$	− 10.76	− 0.36	SHW$_7$	− 2.19	− 0.20
SHW$_{19}$	− 2.97	− 0.28	OPW$_3$	− 5.66	− 0.41
DPW$_{16}$	− 6.42	− 1.14	SHW$_{21}$	− 4.48	− 0.20
SHW$_8$	− 4.21	− 0.40	OPW$_1$	− 10.86	− 0.27
SHW$_{26}$	− 6.70	− 0.31	SHW$_{25}$	− 1.90	− 0.09
SHW31	− 13.56	− 0.45	SHW35	− 13.06	− 0.33
DPW20	− 5.66	− 0.35	SHW$_{39}$	− 36.79	− 0.54
HDW2	− 11.72	− 0.31	SHW43	− 2.94	− 0.23
SP$_{18}$	− 7.22	− 0.50	OPW$_8$	− 6.29	− 0.23
HDW$_{13}$	− 6.15	− 0.36	OPW$_7$	− 11.83	− 0.74
SHW32	− 8.13	− 0.24	HDW$_{10}$	− 4.07	− 0.21
SHW36	− 23.09	− 0.43	SHW$_3$	− 11.99	− 0.22
SP23	− 14.93	− 0.28	SHW48	− 5.81	− 0.21
SP$_{24}$	− 17.04	− 0.27	SP20	− 31.44	− 0.93
SHW$_{37}$	− 33.24	− 0.27	SHW40	− 2.49	− 0.22
SHW$_{38}$	− 79.05	− 0.39	DPW19	− 2.57	− 0.22

and silicate weathering (Gning et al. 2017; Ibrahim et al. 2019; Kumar 2014; Mukherjee et al. 2008).

c) A binary plot and analysis of $SO_4^{2+} + HCO_3^-$ versus $Mg^{2+} + Ca^{2+}$ was done to evaluate the effect of carbonate and silicate weathering on the evolution of groundwater chemistry (Datta and Tyagi 1996; Behera et al. 2019; Pradhan et al 2022). As per the objective of the work, the following binary plot analysis was done:

d) The binary plots of Na^+ versus HCO_3^- and HCO_3^- versus $Na^+ + Cl^-$ were done to evaluate the degree of silicate weathering in the groundwater rock interaction.

e) Binary of Ca versus SO4, Ca versus HCO3$^-$, and $Ca^{2+} + Mg^{2+}$ versus HCO3$^-$ were also done to see the main sources of calcium.

f) Further binary plot analysis of Ca + Mg versus Na was done to identify the type of cation exchange groundwater–aquifer interaction.

g) The binary plot of nitrate versus chloride was performed to examine the anthropogenic effect on groundwater chemistry.

Chloro-alkaline indices (I and II)

Cation exchange is one of the most common hydrogeochemical processes of water–rock interactions in groundwater, which controls the ionic components of groundwater (Xiao et al. 2012). Hence, the chloro-alkaline indices (I and II) were performed to identify the cation exchange which is occurring during the interaction between the groundwater and its host environment while residence or travel. The chloro-alkaline indices were calculated using the following equations (Schoeller 1977):

$$CAI - I = \frac{Cl^- - (Na^+ + K^+)}{Cl^-} \tag{1}$$

$$CAI - II = \frac{Cl^- - (Na^+ + K^+)}{HCO_3^- + SO_4^{2-} + CO_3^{2-} + NO_3^-} \tag{2}$$

where the concentration of ions is in meq/l.

Base exchange index (BEX

The Base Exchange index (BEX) analysis was done to assess the exchange of water between groundwater and seawater which in turn was used to infer the origin of groundwater in the basin as the terrain and the groundwater-bearing formation are mainly sedimentary. This analysis is performed as the sum cations, such as Na^+, K^+, and $Mg2^+$ (in meq/L), corrected for a contribution of sea salt, which assumes the absence of other sources (Pieter 1999), and is given as:

Table 4 Saturation indices of major minerals and Base Exchange Index (BEX) of the Samples

Sample code	Anhydrite	Aragonite	Calcite	Dolomite	Gypsum	Halite	Sylvite	BEX
SP$_1$	− 3.5	− 1.01	− 0.86	− 1.69	− 3.13	− 8.8	− 7.54	6.24
SP$_6$	− 3.5	− 1.01	− 0.86	− 1.69	− 3.13	− 8.8	− 7.54	8.41
OPW2	− 3.4	− 0.86	− 0.71	− 1.33	− 3.03	− 8.64	− 7.62	7.43
SHW$_{18}$	− 3.31	0.06	0.2	0.58	− 2.99	− 8.56	− 7.53	10.22
SHW$_{19}$	− 2.52	0.62	0.77	1.57	− 2.18	− 8.16	− 7.07	10.10
DPW$_{16}$	− 2.43	1.01	1.16	2.5	− 2.14	− 7.1	− 6.85	15.47
SHW$_8$	− 3.21	− 0.6	− 0.45	− 0.78	− 2.82	− 8.21	− 6.83	15.76
SHW$_{26}$	− 2.99	0.39	0.53	1.23	− 2.68	− 8.17	− 7.43	11.70
SHW31	− 2	− 1.03	− 0.88	− 1.63	− 1.67	− 7.93	− 7.18	13.08
DPW20	− 1.9	0.11	0.25	0.69	− 1.59	− 7.57	− 7.49	11.05
HDW2	− 3.29	− 0.71	− 0.57	− 1.17	− 2.91	− 8.63	− 7.49	7.77
SP$_{18}$	− 3.08	− 0.41	− 0.26	− 0.46	− 2.72	− 7.67	− 7.29	11.27
HDW$_{13}$	− 3.18	0.69	0.83	1.84	− 2.87	− 8.77	− 727	12.30
SHW32	− 3.14	− 0.58	− 0.43	− 0.65	− 2.81	− 8.57	− 7.64	11.03
SHW36	− 3.09	− 0.88	− 0.73	− 1.96	− 2.72	− 8.73	− 7.44	5.96
SP23	− 3.67	− 1.14	− 1	− 1.68	− 3.31	− 8.8	− 7.88	5.64
SP$_{24}$	− 35	− 1.19	− 1.04	− 2.13	− 3.16	− 8.73	− 7.88	4.49
SHW$_{37}$	− 3.49	− 1.25	− 1.11	− 2.22	− 3.15	− 9.28	− 8.3	3.5
SHW$_{38}$	− 3.45	− 1.03	− 0.88	− 1.29	− 3.11	− 8.83	− 8.02	10.07
HDW$_{18}$	− 3.54	− 1.11	− 0.97	− 1.75	− 3.2	− 9.09	− 8.05	6.23
SP$_{12}$	− 3.24	− 0.11	0.03	0.3	− 2.92	− 8.94	− 7.68	8.38
SHW$_6$	− 3.34	− 1.22	− 1.07	− 1.98	− 2.99	− 8.26	− 7.25	12.19
SHW$_7$	− 3.05	− 1.21	− 1.06	− 2.1	− 2.71	− 8.01	− 7.32	10.01
OPW$_3$	− 3.14	− 0.54	− 0.39	− 0.69	− 2.78	− 8.14	− 7.33	10.12
SHW$_{21}$	− 2.95	1.45	1.6	2.77	− 2.63	− 7.76	− 7.18	5.16
OPW$_1$	− 3.3	− 0.81	− 0.66	− 1.2	− 2.93	− 9.42	− 7.66	8.74
SHW$_{25}$	− 3.15	0.08	0.23	0.49	− 2.82	− 8.76	− 7.45	8.87
SHW35	− 3.41	− 1.16	− 1.02	− 1.78	− 3.03	− 9.15	− 7.85	6.9
SHW$_{39}$	− 3.67	− 1.12	− 0.98	− 1.62	− 3.33	− 8.57	− 8.08	8.36
SHW43	− 3.1	0.51	0.66	1.54	− 2.8	− 8.13	− 7.53	8.59
OPW$_8$	− 2.78	− 0.03	0.11	0.34	− 2.46	− 8.55	− 7.55	9.68
OPW$_7$	− 2.97	− 0.71	− 0.56	− 1.05	− 2.64	− 7.7	− 7.16	11.53
HDW$_{10}$	− 2.88	1.3	1.4	2.93	− 2.57	− 8.04	− 7.19	9.14
SHW$_3$	− 3.11	− 1.09	− 0.94	− 1.88	− 2.75	− 8.64	− 8.02	6.9
SHW48	− 2.5	0.62	0.77	1.65	− 2.2	− 8.51	− 7.51	6.16
SP20	-3.05	− 0.33	− 0.19	− 0.42	− 2.74	− 8.1	− 7.56	10.18
SHW40	− 3.08	0.32	0.46	0.69	− 2.79	− 7.48	0	3.43
DPW19	− 2.09	− 0.4	− 0.26	− 1.16	− 1.77	− 7.44	0	2.37

$$BEX = [Na + K + Mg) − 1.0716Cl \qquad (3)$$

From this analysis, the positive values of BEX revealed the base flow from the groundwater to the sea and are freshening process. The negative value of BEX indicates the salinization of groundwater where the seawater flows to the groundwater zone, but the zero value of BEX is an indication of an equilibrium circumstance where there is balancing (Stuyfzand 1993).

Saturation index calculation

The saturation index calculation was done using the PHREEQC interactive software program, which was used to interpret and evaluate the further tendency of interaction between the aquifer material and the water (Parkhurst 1995). This analysis is popularly used to understand the degree of equilibrium between mineral species and water. The changes in the state of saturation of the dominant minerals in water are

Table 5 Double Chemical Analysis Results of Cations

Code	Location		Ca^{2+}			Mg2 +			Na$^+$			K$^+$		
	Easting	Northing	1st	2nd	D/ce	1st	2nd	D/ce	1st	2nd	D/ce	1st	2nd	D/ce
SP$_1$	566,929	1,494,072	72	72.5	− 0.5	42	42	0	14	13.6	0.4	88	88	0
SP$_6$	562,357	1,492,490	153	152.6	0.4	78	78.3	− 0.3	22	22	0	43	43.6	− 0.6
OPW2	556,984	1,490,616	90	89.2	0.8	60	60	0	19	19	0	68	68.5	− 0.5
SHW$_{18}$	551,337	1,497,369	140	141.2	− 1.2	98	98.1	− 0.1	16	16.2	− 0.2	61	60.7	0.3
SHW$_{19}$	551,788	1,498,876	192	191.2	0.8	102	102.6	− 0.6	14	14	0	62	62	0
DPW$_{16}$	550,688	1,498,802	178	178	0	120	120	0	106	106.8	− 0.8	70	70	0
SHW$_8$	545,028	1,501,772	216	216.7	− 0.7	160	159.8	0.2	12	12	0	99	99.6	− 0.6
SHW$_{26}$	547,182	1,495,538	173	172.2	0.8	116	116	0	25	25	0	50	49.8	0.2
SHW31	545,149	1,494,325	168	168.8	− 0.8	109	109.5	− 0.5	45	44.5	0.5	92	92	0
DPW20	551,578	1,492,548	146	146	0	99	99	0	61	60.8	0.2	27	27	0
HDW2	552,130	1,496,461	135	134.6	0.4	68	68.7	− 0.7	14	13.6	0.4	66	66	0
SP$_{18}$	543,697	1,496,565	165	165.6	− 0.6	98	98.6	− 0.6	55	55	0	46	45.6	0.4
HDW$_{13}$	545,633	1,496,957	178	177.4	0.6	120	120	0	8	8	0	92	91.5	0.5
SHW32	548,725	1,492,253	146	146.7	− 0.7	113	113	0	15	15.6	− 0.6	46	46	0
SHW36	564,126	1,490,202	205	204.1	0.9	34	39.6	− 5.6	15	14.8	0.2	102	102.4	− 0.4
SP23	568,959	1,492,419	45	45	0	48	47.7	0.3	15	15	0	43	43	0
SP$_{24}$	560,255	1,496,693	72	72.6	− 0.6	32	32	0	18	18	0	45	45	0
SHW$_{37}$	574,181	1,493,850	50	50.3	− 0.3	24	24.5	− 0.5	12	12.6	− 0.6	40	39.6	0.4
SHW$_{38}$	572,695	1,494,176	53	53.6	− 0.6	78	78	0	36	35.6	0.4	80	79.5	0.5
HDW$_{18}$	572,812	1,490,526	64	63.6	0.4	48	48	0	16	16	0	62	62	0
SP$_{12}$	557,330	1,495,628	90	90	0	72	71.6	0.4	12	12	0	77	76.8	0.2
SHW$_6$	550,149	1,500,312	164	164.8	− 0.8	120	120.6	− 0.6	19	18.8	0.2	67	67.8	− 0.8
ShW$_7$	544,949	1,502,029	206	205.9	0.1	106	106	0	20	19.8	0.2	35	35	0
OPW$_3$	548,095	1,499,303	153	153.6	− 0.6	98	97.7	0.3	23	23.6	− 0.6	52	53	− 1
ShW$_{21}$	543,935	1,498,066	196	196	0	34	34	0	37	37	0	50	50.6	− 0.6
OPW$_1$	556,482	1,490,675	123	122.3	0.7	87	87.6	− 0.6	3	3.6	− 0.6	59	58.8	0.2
SHW$_{25}$	544,196	1,495,952	186	185.2	0.8	98	98.5	− 0.5	5	4.8	0.2	36	36	0
SHW35	569,552	1,490,521	67	67	0	66	66	0	7	7	0	47	46.8	0.2
ShW$_{39}$	572,083	1,490,503	64	64	0	68	68	0	39	39.6	− 0.6	42	41.6	0.4
SHW43	556,707	1,496,957	120	119.6	0.4	89	89.6	− 0.6	20	20	0	29	29	0
OPQ$_8$	548,785	1,493,446	163	162.6	0.4	98	97.5	0.5	13	13.6	− 0.6	47	46.8	0.2
OPW$_7$	545,232	1,496,026	154	154	0	87	86.5	0.5	62	62	0	77	76.8	0.2
HDW$_{10}$	542,742	1,496,928	176	176.6	− 0.6	87	87.6	− 0.6	22	22	0	56	56	0
SHW$_3$	556,481	1,490,737	125	124.8	0.2	65	65.4	− 0.4	20	19.8	0.2	29	29.6	− 0.6
SHW48	554,141	1,495,331	98	98.3	− 0.3	56	56	0	13	13.6	− 0.6	47	47.4	− 0.4
SP20	545,556	1,493,347	166	166	0	68	68	0	62	62	0	77	77.6	− 0.6
SHW40	544,459	1,496,518	187	187.2	− 0.2	88	87.6	0.4	22	22	0	53	53	0
DPW19	548,895	1,493,433	158	158	0	76	76.7	− 0.7	8	7.8	0.2	56	56	0

helpful in providing significant information on the hydrogeochemical processes which govern the groundwater chemistry (Belkhiri et al. 2012; Behera et al. 2019; Pradhan et al 2022). The saturation index of a mineral is calculated by the following equation (Deutsch 1998).

$$SI = log \frac{IAP}{Kmineral} \qquad (4)$$

where, SI = saturation index, IAP = ion activity product of the dissociated chemical species in solution, and Kmineral = the solubility constant of the mineral. When SI > 0, the specific mineral is oversaturated and precipitation is possible; when SI = 0, the specific mineral is in equilibrium with the solution, and when SI < 0, the specific mineral is undersaturated and dissolution is possible.

Table 6 Double Chemical Analysis Results of Anions

| Sample Code | Location | | PO_3^{2-} | | | NO_3^{2-} | | | SO_4^{2-} | | | Cl^- | | HCO_3^- |
Sample	Easting	Northing	1st	2nd	D/ce	353.8	2nd	D/ce	1st	2nd	D/ce	1st	2nd	353.8
SP_1	566,929	1,494,072	45.65	43.88	1.77	311.1	1.202	− 0.154	3.2	3.4	− 0.2	4.2	4	311.1
SP_6	562,357	1,492,490	30.44	28.65	1.79	457.5	0.446	− 0.005	2.3	2.1	0.2	4.9	5	457.5
OPW2	556,984	1,490,616	3.956	3.857	0.099	347.7	0.494	− 0.039	3.7	3.7	0	4.6	5	347.7
SHW_{18}	551,337	1,497,369	22.12	20.03	2.09	329.4	1.055	− 0.024	3.3	3	0.3	6.8	7	329.4
SHW_{19}	551,788	1,498,876	17.14	19.11	− 1.97	268.4	0.781	− 0.046	16.9	17.1	− 0.2	19.6	20	268.4
DPW_{16}	550,688	1,498,802	27.2	26.61	0.59	359.9	0.351	0.015	22.3	22	0.3	30.6	31	359.9
SHW_8	545,028	1,501,772	29.49	28.66	0.83	390.4	7.464	− 0.198	4	4	0	20.8	21	390.4
SHW_{26}	547,182	1,495,538	30.65	29.95	0.7	457.5	1.671	− 0.107	6.2	5.8	0.4	10.9	11	457.5
SHW31	545,149	1,494,325	20.12	20.21	− 0.9	378.2	0.174	0.014	65	65	0	10.5	11	378.2
DPW20	551,578	1,492,548	94.29	93.87	0.42	402.6	8.292	− 0.147	85.5	84.8	0.7	17.8	18	402.6
HDW2	552,130	1,496,461	22.07	20.78	1.29	366	10.23	− 0.632	3.6	3.6	0	6.4	6	366
SP_{18}	543,697	1,496,565	22.95	22.41	0.54	384.3	7.981	− 0.146	5.4	5.8	− 0.4	15.4	15	384.3
HDW_{13}	545,633	1,496,957	25.31	23.86	1.45	408.7	9.261	− 0.559	4	3.8	0.2	13.4	13	408.7
SHW32	548,725	1,492,253	23.59	23.59	0	433.1	7.313	0.253	5.1	4.7	0.4	7.1	7	433.1
SHW36	564,126	1,490,202	15.14	16.06	− 0.92	347.7	2.153	0.517	3.8	4.1	− 0.3	4.8	5	347.7
SP23	568,959	1,492,419	16.99	17.56	− 0.57	402.6	10.8	− 0.12	3.2	2.9	0.3	3.9	4	402.6
SP_{24}	560,255	1,496,693	22.75	24.85	− 2.1	329.4	1.112	− 0.034	2.9	3.1	− 0.2	3.8	4	329.4
SHW_{37}	574,181	1,493,850	94.58	94.29	0.29	542.9	0.82	− 0.063	3.7	3.2	0.5	1.6	2	542.9
SHW_{38}	572,695	1,494,176	20.85	21.32	− 0.47	372.1	6.861	− 0.066	5.5	5	0.5	1.6	2	372.1
HDW_{18}	572,812	1,490,526	22.12	23.08	− 0.96	396.5	1.471	− 0.254	3.1	3.2	− 0.1	1.9	2	396.5
SP_{12}	557,330	1,495,628	51.32	52.12	− 0.8	390.4	1.202	0.446	5.1	5.1	0	3.7	4	390.4
SHW_6	550,149	1,500,312	28.51	30.61	− 2.1	353.8	7.195	− 0.114	3.1	4	− 0.9	11.7	12	353.8
SHW_7	544,949	1,502,029	20.26	19.89	0.37	280.6	2.316	− 0.099	4.8	5.2	− 0.4	19.6	20	280.6
OPW_3	548,095	1,499,303	39.06	40.002	− 0.94	701.5	7.474	− 0.078	4.8	4.6	0.2	12.4	12	701.5
SHW_{21}	543,935	1,498,066	23.97	26.61	− 2.64	329.4	10.21	− 9.239	5.3	5.1	0.2	18.7	19	329.4
OPW_1	556,482	1,490,675	28.08	28.61	− 0.53	481.9	4.84	− 0.006	3.9	3.9	0	4.9	5	481.9
SHW_{25}	544,196	1,495,952	17.97	18.64	− 0.67	244	1.324	0.016	4	3.8	0.2	13.9	14	244
SHW35	569,552	1,490,521	22.61	23.23	− 0.62	298.9	8.655	0	4.5	4.2	0.3	3.8	4	298.9
SHW_{39}	572,083	1,490,503	2.49	2.93	− 0.44	308.66	1.201	0.028	2.5	2.5	0	2.6	3	308.66
SHW43	556,707	1,496,957	20.68	21.23	− 0.55	384.3	2.73	− 0.27	5.6	5.2	0.4	14.5	15	384.3
OPW_8	548,785	1,493,446	22.22	23.12	− 0.9	347.7	0.877	− 0.155	10	10.3	− 0.3	8.6	9	347.7
OPW_7	545,232	1,496,026	24.71	26.46	− 1.75	536.8	0.243	0.022	6.8	7.2	− 0.4	12.9	13	536.8
HDW_{10}	542,742	1,496,928	24.27	23.87	0.4	402.6	7.527	− 0.437	7.6	7.9	− 0.3	16.7	17	402.6
SHW_3	556,481	1,490,737	33.98	34.25	− 0.27	396.5	6.714	0.037	5.5	6.2	− 0.7	4.4	4	396.5
SHW48	554,141	1,495,331	28.76	30.17	− 1.41	285.48	9.197	− 0.097	23.9	24.3	− 0.4	9.2	9	285.48
SP20	545,556	1,493,347	32.24	31.65	0.59	433.1	5.22	− 0.82	4.8	4.1	0.7	5.1	5	433.1
SHW40	544,459	1,496,518	94.04	93.41	0.63	384.3	6.802	0.025	5.8	4.2	1.6	23.4	25	384.3
DPW19	548,895	1,493,433	92	92.34	0.34	HCO_3^-	10.0	− 0.5	65.2	65.9	0.7	24.2	24.9	353.8

Results

Physico-chemical parameters

The in situ and laboratory analysis results for the cations, anions, and other chemical parameters of the groundwater samples have been compiled (Table 1). The pH in the groundwater ranges between 5.71 and 8.1, recording in SHW_7 and HDW_{10} respectively (Table 1) and about 68.42%

of the groundwater samples revealed a pH value ranging from 5.71 to 6.9, which indicates that the groundwater in the catchment is non- alkaline nature. The pH values show an incremental from eastern, southern, and northern toward the western part of the catchment. The temperature of the groundwater samples ranges from 17.5 to 25.8 ℃. The maximum value was recorded in SP_6 from the lower catchment whereas the minimum value was recorded in SHW_{40} from the upper catchment.
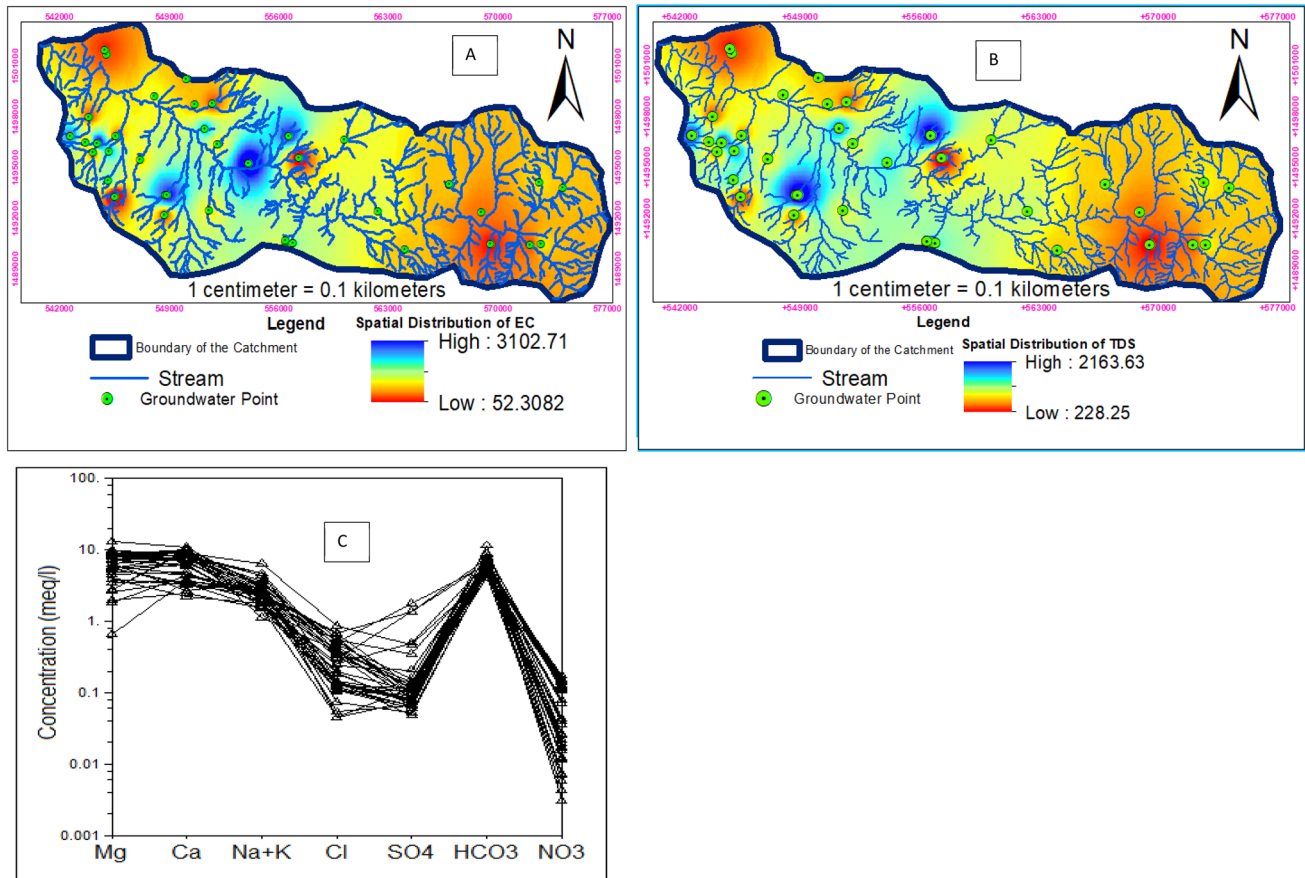
Fig. 3 **A** Spatial Distribution of EC **B** Spatial Distribution of TDS **C** Groundwater samples on a Schoeller Diagram

The groundwater samples from the catchment indicate a wide range of electrical conductivity (Table 1), ranging from 50 μs/cm (SP_{20}) to 3121 μs/cm (SHW_{40}) and this indicates the water quality varies from fresh to saline groundwater. From the spatial distribution diagram of EC (Fig. 3A), it was observed that the EC value is increased from the recharge at the east toward the discharge in the western part of the catchment. It is observed that the EC distribution is parallel to the groundwater flow path where significant anomalies are recorded surrounding the city and close to the industries (Fig. 3A). The degree of salinity of the groundwater increases along the general groundwater flow direction, from the eastern to western. The liquid and solid wastes released from the city and the industries could be responsible for the high value of the EC in the catchment but, the aquifer material contribution is also significant.

Concentrations of Mg^{2+}, Ca^{2+}, Na^+ and K^+ are ranging from 8 to 160 mg/l, 45 to 216 mg/l, 3 to 106 mg/l and 0 to 120 mg/l respectively. Concentrations of HCO_3^-, PO_4^{3-}, Cl^-, SO_4^{2-} and NO_3^- vary from 244 to 701.5 mg/l, 2.5 to 94.6 mg/l, 1.6 to 30.6 mg/l, 2.3 to 85.5 mg/l and 0.2 to 10.7 mg/l respectively. The minimum and maximum values for total dissolved solids in the catchment are 228.205 mg/l

(SP_{12}) and 2175.08 mg/l (DPW_{19}) respectively (Table 1). The TDS value revealed a generally increasing trend from the eastern to the western part of the catchment parallel to the groundwater flow path (Fig. 3B), with a high concentration around the city and adjacent to the industrial zones, which has a similar fashion to the EC spatial distribution. This confirms that EC is controlled by TDS, where highly mineralized water is more conductor than water with low concentration, and hence, the salinity of the water is increased as one goes from the eastern to the western of the catchment under investigation. The waste materials and chemicals that are discharged from the city and the small-scale industries could be the ground sources in addition to the effect of the aquifer materials.

The nitrate concentration in the groundwater samples ranges from 0.188 mg/l (SHW_{31}) to 9.5 mg/l (DPW_{19}) (Table 1) and more than 76% of groundwater samples revealed that much more than the natural concentration of this ion, which is generally less than 1 mg/l (Agrawal et al. 1999). In contrast to this, the nitrate concentration in the groundwater samples is more exaggerated than the natural background of the ion and the significant concentration of this shows an anthropogenic source of nitrate. The phosphate

concentration in the groundwater samples ranges from 2.4 mg/l (SHW39) to 94.6 mg/l (SHW37) with an average of 30.3 mg/l (Table 1). The main sources of phosphate in groundwater are overlying soil, dissolution of phosphate-bearing minerals in the aquifer, agricultural fertilizer, animal waste, and leaking septic systems or infiltration of wastewater (Fuhrer et al. 1999). In this catchment, phosphate-bearing sediments have not been reported yet, so that, the sources for the high concentration of phosphate in groundwater are mainly related to anthropogenic activities such, as fertilizer and wastes, from the city and industries.

Discussion

Ionic dominance and groundwater facies

To identify the dominant ions in the groundwater and hence the groundwater facies, both the cations and anions

of the groundwater samples were plotted on the Schoeller diagram (Schoeller 1955) and Piper diagram (Piper 1944). The dominant major ions in the groundwater in descending order are Ca^{2+}, Mg^{2+}, Na^+, and K^+ and HCO_3^-, PO_4^{3-}, $SO4^{2-}$, Cl^-, and NO_3^- for cations and anions, respectively (Table 1; Fig. 3C & 4a). Bicarbonate is the dominant anion for all groundwater samples (Fig. 4a), which is possibly due to the carbonate material weathering and dissolution of carbonate minerals. Even though almost all the groundwater samples are plotted in the bicarbonate dominant type in the case of cations, the concentration of calcium and magnesium is much higher than sodium and potassium (Fig. 4a). As shown in Fig. 4a, the groundwater facies in the catchment is predominantly Ca-Mg-HCO3 and Mg-Ca-HCO3 (Fig. 4a) types and this is consistence with the dominance of calcium, magnesium, and bicarbonate components (Table 2. Generally, the trends in the Schoeller diagram are the same for all samples and this suggests a common source, and needs further analysis which will be addressed in the following sections.
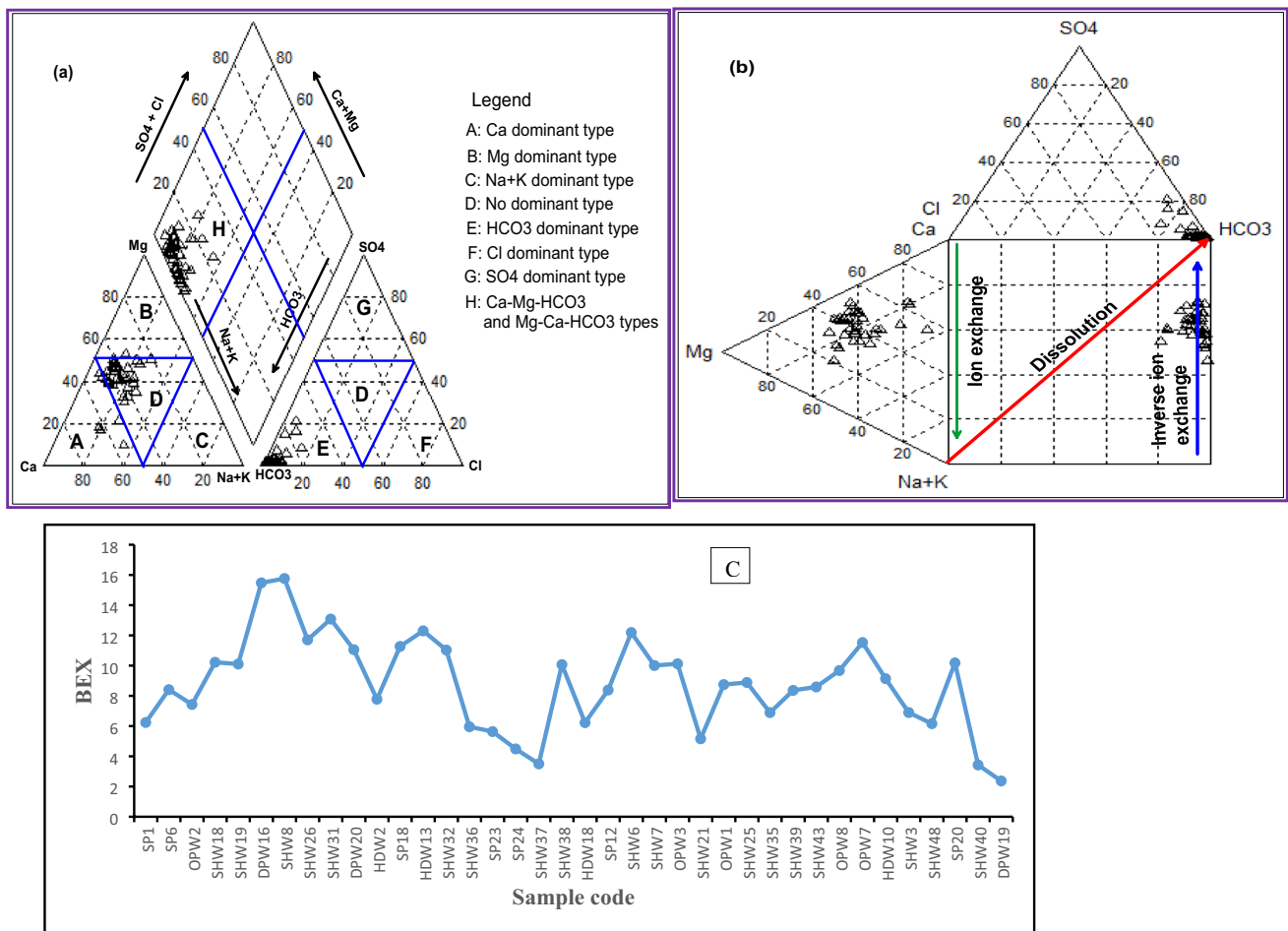

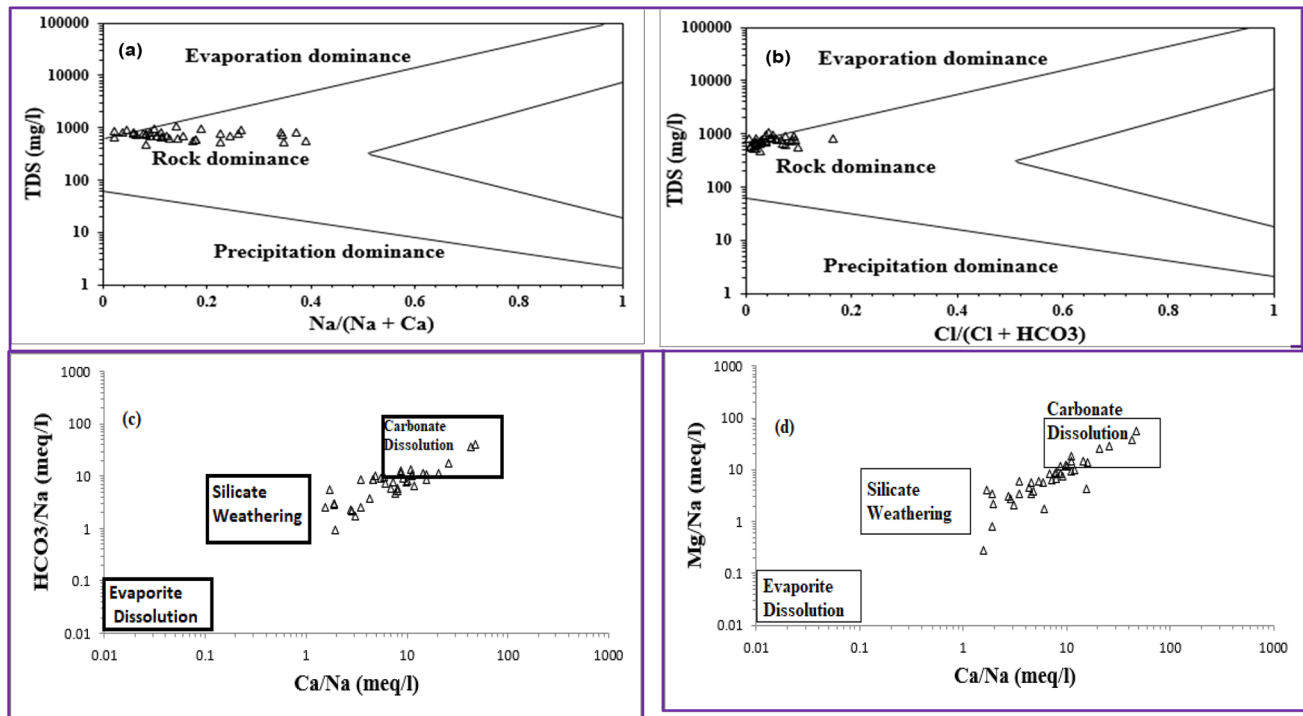**Fig. 4** Groundwater Facies and BEX **a** Piper Plot **b** Durov **c** Base Exchange index (BEX)

Fig. 5 Ionic Binary plots **a** Na/(Na+Ca)versus TDS **b** Cl/(Cl+HCO3) versus TDS **c** Ca/Na versus HCO3/Na) Ca/Na versus Mg/Na

Rock–water interaction

As per the binary plots of TDS versus Na/ (Na+Ca) and TDS versus Cl/ (Cl+HCO3) (Fig. 5a & b), the groundwater samples are plotted dominantly toward the rock dominance zone, which implies the rock–water interaction is the main governing factor for the evolution of groundwater chemistry in the catchment. Dissolution, such as carbonate dissolution, evaporate dissolution and silicate weathering are components in the rock–water interaction domain (Gning et al. 2017; Ibrahim et al. 2019; Kumar 2014; Mukherjee et al. 2008). Further, the binary plot analysis of Ca/Na versus HCO3/Na and Ca/Na versus Mg/Na (Fig. 5c & d), was performed to identify the component of rock interaction which is contributed as a main natural process involved in changing groundwater chemistry. Accordingly, most of the groundwater samples are plotted from the end zone of silicate weathering toward the carbonate dissolution, which reveals carbonate dissolution is the major geochemical process that controls the evolution of groundwater chemistry in the catchment (Fig. 5c, d). The sources of major ions in the groundwater and their evolution mechanisms can be identified from the compositional relations of the dissolved species (Fisher and Mullican 1997). Hence, the analysis of binary plots of the major ions has been discussed in the following sections.

Further from the scatter plot of $SO_4^{2+} + HCO_3^-$ versus $Mg^{2+} + Ca^{2+}$, most of the samples are plotted below the 1:1 line toward the Ca^{2+} and Mg^{2+} side, and four samples fall in the silicate weathering zone (Fig. 6c). This indicates that the major hydrogeochemical process occurring in the catchment is dominantly by carbonate dissolution (calcite and dolomite) with some extent of silicate weathering. From the cation–anion binary plots, most of the groundwater samples are plotted close to the 1:1 line in the Ca^{2+} versus HCO_3^- plot (Fig. 6a), hence, the dominance of carbonate dissolution for the evolution of groundwater chemistry is also confirmed from this binary plot. In the Mg^{2+} versus Ca^{2+} plot (Fig. 6d), almost all of the groundwater samples fall very close to the 1:1 line, reflecting the concentration of the calcium and magnesium is more or less equal in almost all groundwater samples. However, the groundwater samples are somewhat far from the 1:1 line and pointing toward the $Ca^{2+} + Mg^{2+}$ side in the case of $Ca^{2+} + Mg^{2+}$ versus HCO_3^- plotted (Fig. 6b), which indicates there are also other sources of magnesium ion in addition to the dissolution of dolomite.

The finding of calcium and magnesium dominance in the groundwater is also confirmed by the plots of Ca^{2+} versus SO_4^{2-} (Fig. 6e) and Mg^{2+} versus SO_4^{2-} (Fig. 6f), where the concentration of calcium and magnesium increase over the sulfate. This idea is also supported by the analysis of saturation indices minerals where calcite and dolomite reflect a similar range of saturation indices (Table 4 and Fig. 8a, c). Furthermore, the groundwater samples are dominantly laid from the 1:1 line pointed toward the bicarbonate in the binary plots of Na^+ versus HCO_3^- and HCO_3^- versus
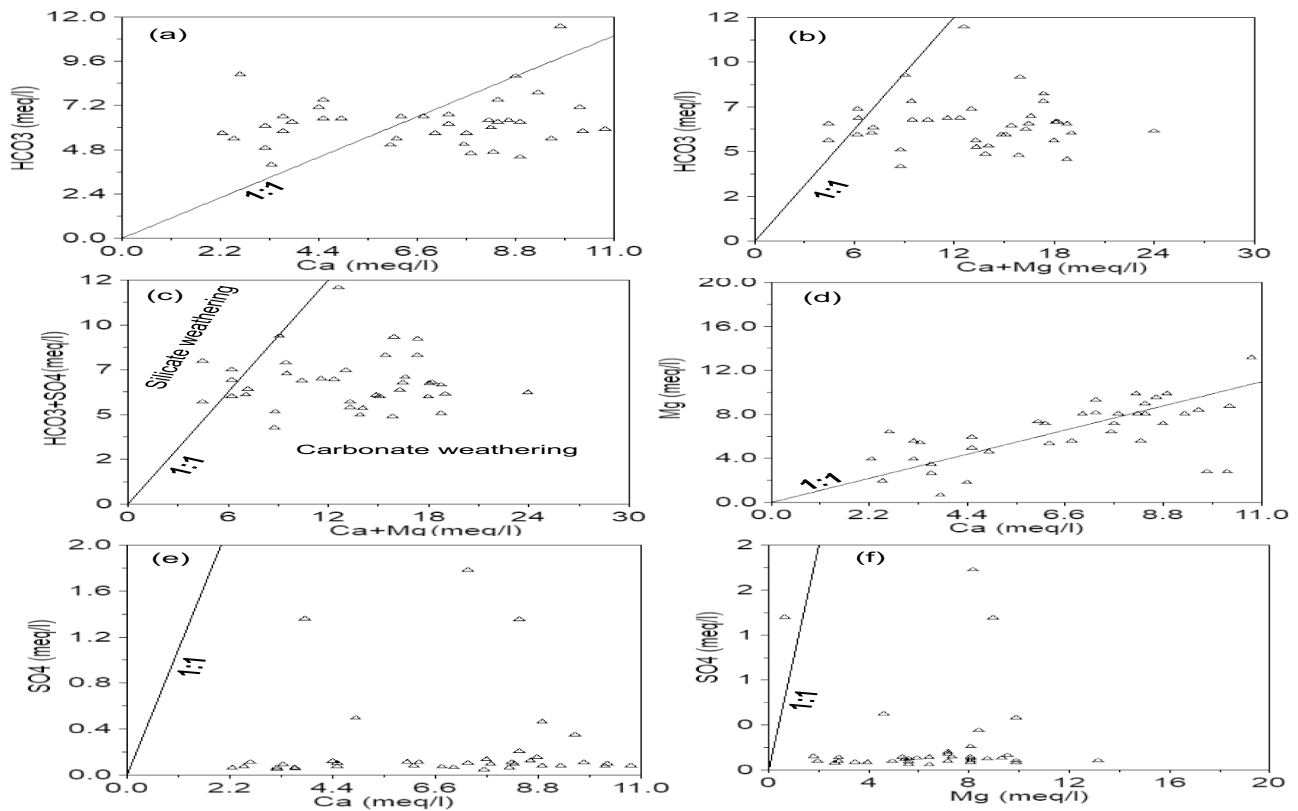
Fig. 6 Ionic binary plots **a** Ca versus HCO3 **b** Ca + Mg versus HCO3 **c** Ca + Mg versus HCO3 + SO4 **d** Ca versus Mg **e** Ca versus SO4 and) Mg versus SO4

$Na^+ + Cl^-$ (Fig. 7a, c) indicating that carbonate weathering is the dominant geochemical process over silicate weathering, involved in the evolution of groundwater chemistry of the catchment. A significant number of the samples are plotted below the equiline toward the sodium dominance in the binary plot of sodium versus chloride (Fig. 7d), which revealed a concentration of sodium ion is much higher than chloride ion. This suggests that silicate weathering or ion exchange also controls the evolution of groundwater chemistry in the catchment. However, there are few samples laid along the equiline, suggesting a common source of halite dissolution for both ions, and few samples plotted above the equiline which indicates a signal of other anthropogenic sources of chloride (Fig. 7d). Furthermore, in the binary diagram of Ca versus SO4 (Fig. 6e), and Ca versus HCO3$^-$ (Fig. 6a) analyses were performed on the groundwater samples in the catchment (SU et al. 2007), and most of them are laid toward the calcium zone from the 1:1 equiline, indicating the dissolution of carbonate minerals (possibly calcite). Since a significant number of samples are plotted above the equilibrium line toward bicarbonate (Fig. 6a), it should be noticed that there are also some limited and common sources for calcium and bicarbonate. Besides, from the $Ca^{2+} + Mg^{2+}$ versus HCO3$^-$ binary plot (Fig. 6b), it was observed that the samples dominantly indicate the high contribution of carbonate dissolution. This shows an excess of calcium over sodium due to reverse ion exchange, but few samples revealed the dominancy of sulfate and bicarbonate over the calcium and magnesium, which are plotted above the equiline, explaining the silicate weathering due to the dolerite intrusion, which also shares the above interpretation (Harrington and Herczeg 2003).

Ion exchange process

The chloro-alkaline indices I & II were calculated using Eqs. 1 and 2. From this calculation, both chloro-alkaline indices I and II are negative for all groundwater samples (Table 3). According to Schoeller (1977), negative values for both indices reflect the presence of a reverse ion exchange process which causes the enrichment of sodium and potassium ions in the groundwater from the aquifer materials and the removal of calcium and magnesium ions from the groundwater to the aquifer materials. Furthermore, binary plot analysis of Ca + Mg versus Na was performed to identify the type of cation exchange that is active in the groundwater (Fig. 7b). Relatively higher concentrations of Ca + Mg over Na in a Ca + Mg versus Na plot show a reverse cation

Fig. 7 Binary plots **a** Na + Cl versus HCO3, **b** Mg + Ca versus Na, **c** Na versus HCO3, **d** Na versus Cl and **e** NO3 versus Cl
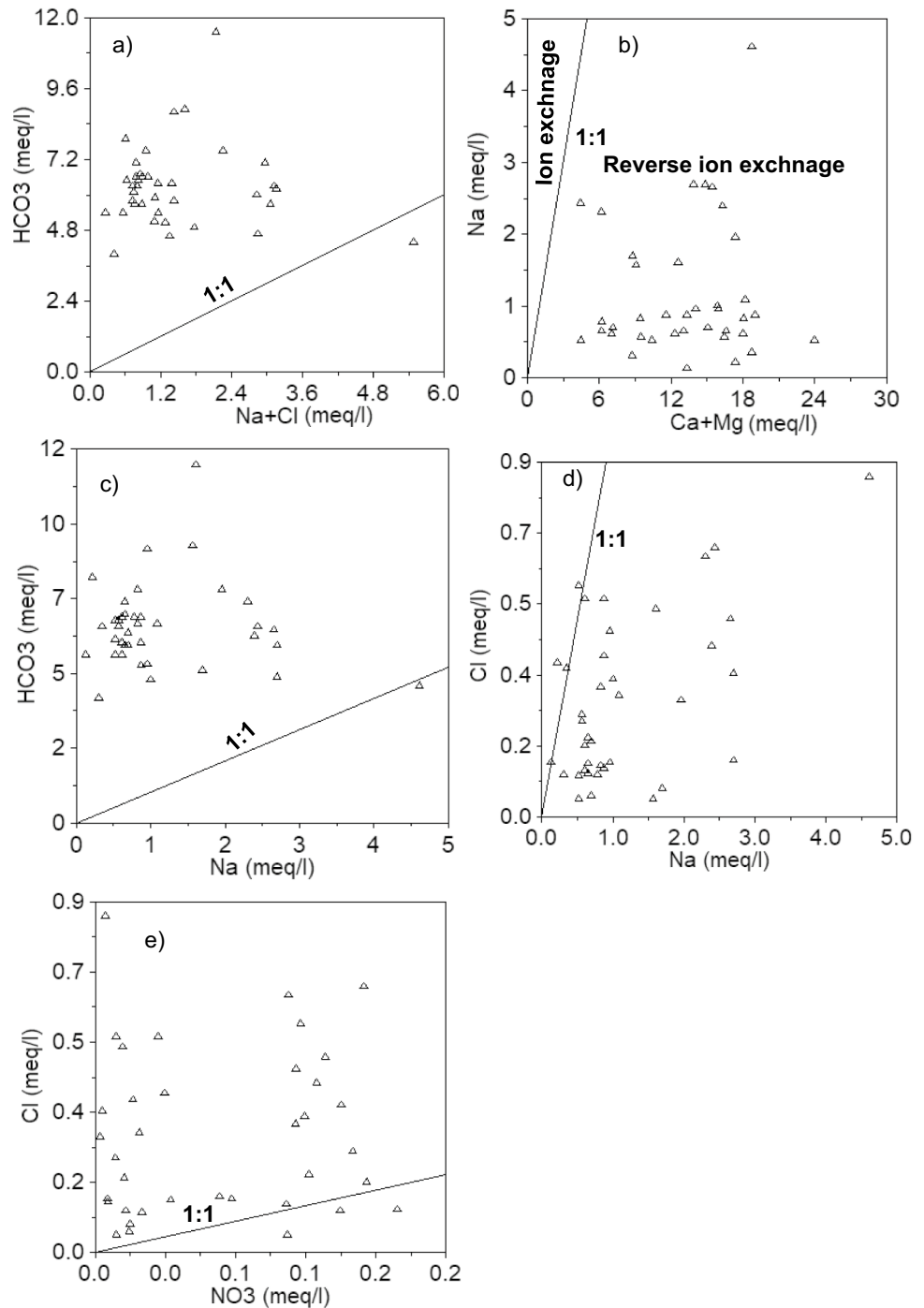
exchange between the groundwater and aquifer materials (Rajmohan and Elango 2004). All of the groundwater samples are plotted below the 1:1 line toward the calcium and magnesium zone, which indicates the presence of reverse ion exchange in the catchment (Fig. 7b). The presence of a shale bed in the aquifer system, which is rich in clay could be the source of sodium and potassium ions in the catchment. The active reverse ion exchange in the groundwater in the catchment is also confirmed by the Durov plot analysis in which all the groundwater samples are laid along the reverse ion exchange zone (Fig. 4b).

The assessment of the Paleo groundwater origin, freshening, and salinization between groundwater and seawater is well examined with the Base Exchange index (BEX) analysis (Stuyfzand 1993). This analysis is important as the catchment is part of the sedimentary basin and groundwater-bearing formations are mainly sedimentary units. In this study, the Base Exchange index was calculated using Eq. 3.
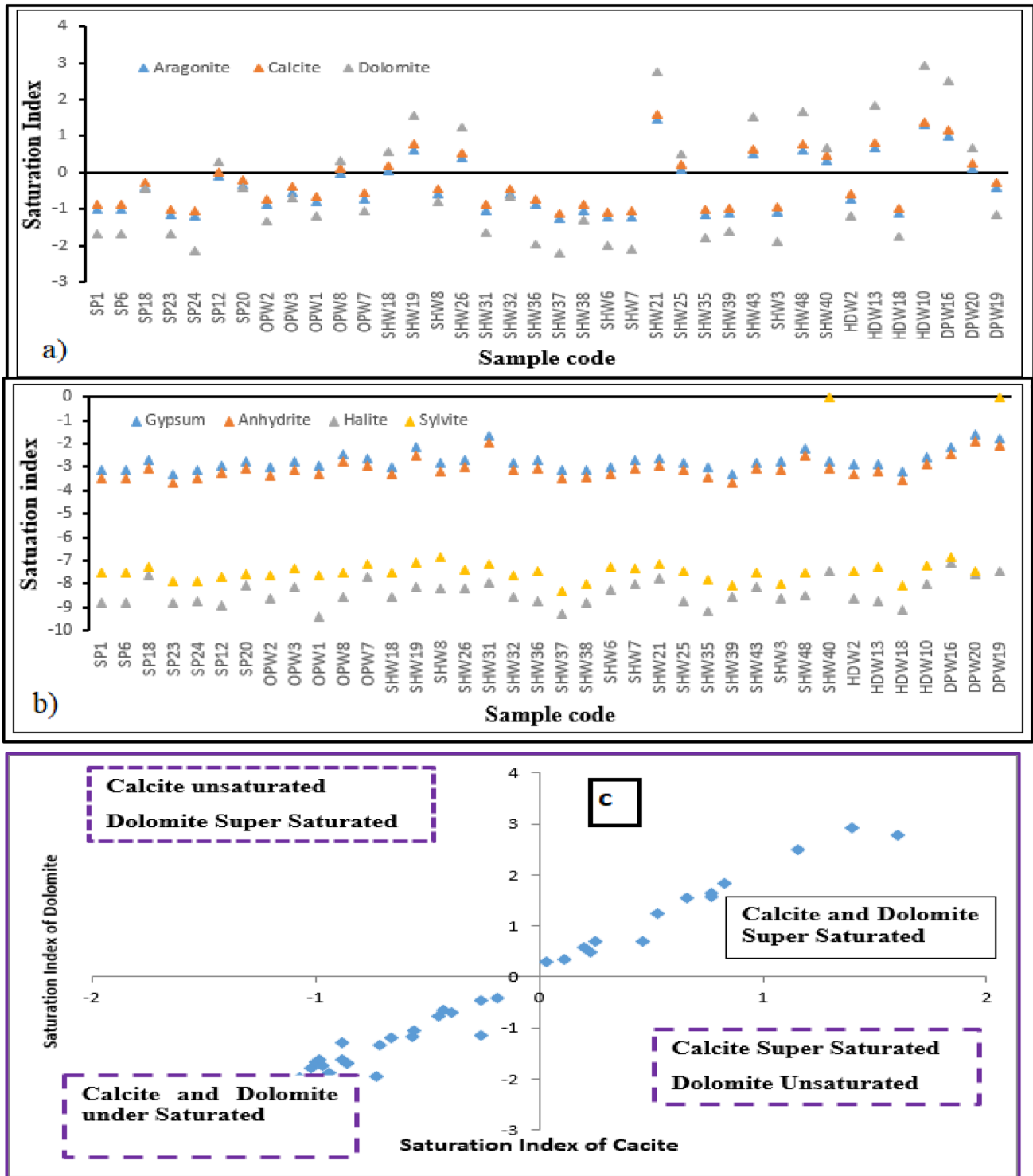
Fig. 8 Saturation Indices of Major Minerals **a** Super Saturated **b** Equilibrium and Under Saturated **c** Saturated Comparison of Calcite and Dolomite

Accordingly, all the groundwater samples revealed a positive Base Exchange index value which is much more than two (Table 4 and Fig. 4c) and is suggested that the groundwater in the catchment is dominated by the meteoritic origin, although it needs further groundwater chemistry study with isotope dating analysis. Moreover, the base-exchange softened water process could be interpreted from the Base Exchange index analysis as far as the high base-exchange

reaction of alkali earth elements exchanged for Na + ion under high concentrations of bicarbonate is over calcium and magnesium (Jeevanandam et al., 2012).

Saturation index of minerals

The saturation index analysis of minerals was done to predict the tendency of mineral dissolution and/or precipitation into the groundwater or to the aquifer materials so that the state of equilibrium between groundwater and the mineral in the aquifer will be identified (Appelo & Postma 2005). Moreover, the result of this analysis is important for the assessment of the nature of the interaction between the groundwater and the minerals of the water-bearing formation, and the current and further geochemical processes that govern the evolution of the groundwater chemistry can be identified. The saturation index of the major minerals of the aquifer materials was calculated using the PHREEQC interactive software program (Table 4 and Fig. 8), and more than 63% of the samples revealed both calcium and magnesium are undersaturated (Fig. 8c). As the groundwater reservoir is dominated by carbonate materials, it is surprising that the groundwater is significantly undersaturated in terms of calcite, dolomite, and aragonite minerals (Fig. 8a, c), which supports the activity of the normal ion exchange between sodium and/or potassium with calcium and/or magnesium, suggesting the parallel dissolution and precipitation reactions occurring in the groundwater. Hence, further dissolution of calcite, dolomite, and aragonite minerals will be possible in the groundwater where the minerals are undersaturated state. Also, the groundwater is entirely found under saturated with a mineral such as halite, sylvite, gypsum, and anhydrite (Table 4 and Fig. 8b), which indicates the further dissolution of these minerals.

Groundwater chemistry along the flow path

The recharge and discharge zones in the catchment are the eastern and western parts of the catchment respectively, which can be identified not only from the surface topography but also from the hydrogeological map of the catchment (Fig. 1D). The spatial distribution of the bicarbonate ratio to chloride (Fig. 4C), confirmed that the groundwater flow in the catchment is from eastern to western, and this indicates dissolution and other hydrochemical processes are significantly strong toward the western part of the catchment, which is supported by the spatial distribution of EC (Fig. 3A) and TDS (Fig. 3B), where their concentration is increased along the groundwater flow path from eastern to western and is higher around Mekelle City and adjacent to the industry in the western part of the catchment. Moreover, the overexploitation of groundwater supply for the city and

the nearby industries can increase the ion concentration in the groundwater in the western part.

Anthropogenic processes

The contaminants induced by human activity termed anthropogenic sources such, as agricultural (animal compost and fertilizer), infiltration of sewerage as well as discharges from septic tanks, and domestic and industrial wastes together with the depletion of groundwater, contributed to the evolution of groundwater chemistry and affecting its quality (Ben Brahim et al. 2012). To examine the impact of anthropogenic activities on groundwater chemistry, binary plots, and the concentration analysis of anthropogenic processes sensitive anions, such as chloride, sulfate, and nitrate, were performed. The binary plot analysis of nitrate versus chloride was performed to investigate the input for these ions (Fig. 7e). Accordingly, it was observed that the ions have derived from different sources, and the animal composts and other fertilizers for agricultural application, and infiltration wastes from sewerage, and septic tanks in addition to the domestic and industrial wastes could be the sources of these ions in the catchment. However, the limited halite input for chloride and the atmospheric sources of nitrate can be also interpreted from the binary analysis of these ions (Fig. 7e). The high concentration of chloride in the drinking water supply leads to toxicity which cannot be sensed in the lower stage of the human body, and is lead even to heart failure (Shahid et al. 2014). Besides, the high level of chloride in the water can cause an increase in electrical conductivity which in turn advances the corrosivity capacity of the water. Moreover, when the water flows in metal pipes and pumps the chloride can react with metal and lead to the addition of metals in the drinking water. Hence, the environmental unfriend application of fertilizers and the poor sewage and waste management system in the area should be addressed to improve the groundwater quality in the area in terms of chloride and nitrate. Since, most of the communities settled away from the mega-cities where the treatment of the groundwater quality gets little attention and the communities are using untreated water, thereby the health risk caused by the nitrate and chloride component in the drinking water is significant from time to which needs to maintain and removal of these anions.

Conclusion

Hydrogeochemical investigations were conducted in the Ellala catchment to understand the main governing factors in the evolution of the groundwater chemistry of the catchment. The groundwater in the catchment is non-alkaline. The pH, TDS, and EC increase from east to west and are significant

around Mekelle City and the industrial zones due to the wastes of the city and the nearby industries, and the degree of salinity of the groundwater indicates a similar fashion with the EC which revealed the direct relationship with TDS. The major ions in descending order are Ca^{2+}, Mg^{2+}, Na^+, and K^+ (cations) and HCO_3^-, PO_4^{3-}, Cl^-, SO_4^{2-} and NO_3^- (anions). Calcium, magnesium, and bicarbonate are the dominant ions in the catchment. Hence, the groundwater of the catchment is predominated by Ca-Mg-HCO3 and Mg-Ca-HCO3 water types.
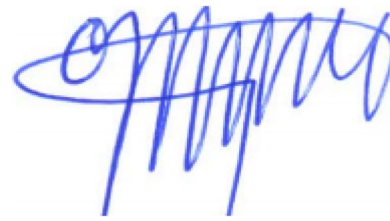
The groundwater chemistry of the catchment is controlled by the rock–water interactions, mainly carbonate dissolution mainly calcite and dolomite, and this idea is supported by saturation indices of minerals where calcite and dolomite revealed a similar range of saturation indices. The reverse cation exchange between the groundwater and aquifer materials is also the dominant geochemical process due to the sodium and potassium ions sources from the presence of a shale bed in the aquifer system, which is rich in clay in the catchment. Although to a limited extent, the silicate weathering due to the dolerite intrusion and halite dissolution from the gypsum layer are also geochemical processes that undergo in the groundwater–aquifer interaction in the catchment. Besides the natural geochemical processes, the groundwater chemistry of the catchment is also modified by anthropogenic activities. The possible source for the high concentration of calcium, magnesium, and bicarbonate in the groundwater is carbonate dissolution. Furthermore, silicate weathering originating from dolerite and other clay minerals is also a source for the enrichment of magnesium ions in the groundwater. The excess concentration of sodium ion over chloride ion is due to reverse ion exchange and/or weathering of sodium-bearing materials, such as shale and dolerite. The sources for the high concentration of phosphate, nitrate, and chloride in the groundwater are mainly anthropogenic activities, sources that need treatment, and groundwater quality control and management in the catchment. The groundwater in the catchment is dominated by the meteoritic origin, although it needs further groundwater chemistry study with isotope dating analysis. The groundwater is undersaturated with calcite, dolomite, and aragonite minerals where further dissolution of these minerals is going in the groundwater.

Data availability The authors declare that the datasets supporting the findings of this article are available within the article itself and its supplementary information files.

Declarations

Conflict of interest statement We the undersigned declare that this manuscript is original, has not been published before, and is not currently being considered for publication elsewhere. We confirm that the manuscript has been read and approved by all named authors and that there are no other persons who satisfied the criteria for authorship but are not listed. We further confirm that the order of authors listed in the manuscript has been approved by all of us. We understand that the corresponding author is the sole contact for the editorial process. He is responsible for communicating with the other authors about progress, submissions of revisions, and final approval of proofs.

Signed by authors.

References

Abid K, Zouari K, Dulinski M, Chkir N, Abidi B (2011) Hydrologic and geologic factors controlling groundwater geochemistry in the Turonian aquifer (southern Tunisia). Hydrogeol J 19(2):415–427. https://doi.org/10.1007/s10040-010-0668-z

Abreha A G (2014) Hydrogeochemical and water quality investigation on irrigation and drinking water supplies in the Mekelle region.

Agrawal GD, Lunkad SK, Malkhed T (1999) Diffuse agricultural nitrate pollution of groundwaters in India. Water Sci Technol 39(3):67–75. https://doi.org/10.1016/S0273-1223(99)00033-5

Ahmed A, Clark I (2016) Groundwater flow and geochemical evolution in the Central Flinders Ranges, South Australia. Sci Total Environ 572:837–851. https://doi.org/10.1016/j.scitotenv.2016.07.123

Aminiyan MM, Aminiyan FM (2020) Comprehensive integrated index–based geochemistry and hydrochemical analyses of groundwater resources for multiple consumptions under coastal conditions. Environ Sci Pollut Res. https://doi.org/10.1007/s11356-020-08300-7

Aminiyan MM, Aminiyan FM, Heydariyan A, Sadikhani MR (2016) The assessment of groundwater geochemistry of some wells in Rafsanjan plain, Iran. Eurasian J Soil Science, 5(3), 221–230. https://doi.org/10.18393/ejss.2016.3.221-230.

Argamasilla M, Barbera JA, Andreo B (2017) Factors controlling groundwater salinization and hydrogeochemical processes in coastal aquifers from southern Spain. Sci. Total Environ. 580, 50e68. https://doi.org/10.1016/j.scitotenv.2016.11.173.

Ayele B, Gangadharan R (2016) Study on geological and structural characterization around Mai Kenetal, Central Tigray in Northern Ethiopia. Int J Eng Appl Sci 3(11):257562

Babiker IS, Mohamed MAA, Hiyama T (2007) Assessing groundwater quality using GIS. Water Resour Manage 21(4):699–715. https://doi.org/10.1007/s11269-006-9059-6

Behera AK, Chakrapani GJ, Kumar S (2019) Identification of seawater intrusion signatures through geochemical evolution of groundwater: a case study based on the coastal region of the Mahanadi delta, Bay of Bengal, India. Nat Hazards 97:1209–1230. https://doi.org/10.1007/s11069-019-03700-6

Belkhiri L, Mouni L, Boudoukha A (2012) Geochemical evolution of groundwater in an alluvial aquifer: case of El Eulma aquifer, East Algeria. J Afr Earth Sc 66–67:46–55. https://doi.org/10.1016/j.jafrearsci.2012.03.001

Ben Brahim F, Khanfir H, Bouri S (2012) Groundwater vulnerability and risk mapping of the Northern Sfax Aquifer, Tunisia. Arab J Sci Eng 37(5):1405–1421. https://doi.org/10.1007/s13369-012-0261-y

Beyth M (1972) Paleozoic-mesozoic sedimentary basin of mekele outlier. Northern Ethiopia AAPG Bulletin 56(12):2426–2439. https://doi.org/10.1306/819A422A-16C5-11D7-8645000102C1865D

Bucci A, Franchino E, Antonio D, Luca D, Lasagna M, Coyoy I M, Osvaldo E, Escobar S A (2017) Journal of South American Earth Sciences Groundwater chemistry characterization using multi-criteria River basin (SW Guatemala) approach : The upper Samal a. 78. https://doi.org/10.1016/j.jsames.2017.07.001.

Ellala Catchment, Tigray, Northern Ethiopia. Momona Ethiopian Journal of Science, 7(2), 203. https://doi.org/10.4314/mejs.v7i2.5.

Choi BY, Yun ST, Kim KH, Kim JW, Kim, HM, Koh YK (2014) Hydrogeochemical interpretation of South Korean groundwater monitoring data using Self-Organizing Maps. J. Geochem. Explor. 137, 73e84. https://doi.org/10.1016/j.gexplo.2013.12.001.

Dehbandi R, Moore F, Keshavarzi B (2018) Geochemical sources, hydrogeochemical behavior, and health risk assessment of fluoride in an endemic fluorosis area, central Iran. Chemosphere 193: 763e776. https://doi.org/10.1016/j.chemosphere.2017.11.021.

Deutsch BWJ (1998) Groundwater geochemistry: fundamentals and applications to contamination. Choice Rev Online, 35(07): 35–3883–35–3883. https://doi.org/10.5860/choice.35-3883.

Fazzini M, Bisci C, Billi P (2015) The Climate of Ethiopia. World Geomorphological Landscapes, 65–87. https://doi.org/10.1007/978-94-017-8026-1.

Fisher RS, Mullican WF (1997) Hydrochemical evolution of sodium-sulfate and sodium-chloride groundwater beneath the Northern Chihuahuan Desert, Trans-Pecos, Texas, USA. In Hydrogeol J (Vol. 5, Issue 2, pp. 4–16). https://doi.org/10.1007/s100400050102.

Gibbs RJ (1970) Mechanisms controlling world water chemistry. Science 170(3962):1088–1090. https://doi.org/10.1126/science.170.3962.1088

Girmay E, Ayenew T, Kebede S, Alene M, Wohnlich S, Wisotzky F (2015) Conceptual groundwater flow model of the Mekelle Paleozoic—Mesozoic sedimentary outlier and surroundings (northern Ethiopia) using environmental isotopes and dissolved ions. 649–672. https://doi.org/10.1007/s10040-015-1243-4.

Gning AA, Orban P, Gesels J, Ngom FD, Dassargues A, Malou R, Brouyère S (2017) Factors controlling the evolution of groundwater dynamics and chemistry in the Senegal River Delta. J Hydrol 10:133–144. https://doi.org/10.1016/j.ejrh.2017.01.005

Grmay K, Nata T, Tesfamichael G (2015) Aquifers Characterization and Productivity in

Güler C, Thyne GD (2004) Hydrologic and geologic factors controlling surface and groundwater chemistry in the Indian Wells-Owens Valley area, southeastern California, USA. J Hydrol 285(1–4):177–198. https://doi.org/10.1016/j.jhydrol.2003.08.019

Harrington GA, Herczeg AL (2003) The importance of silicate weathering of a sedimentary aquifer in arid Central Australia is indicated by very high 87Sr/86Sr ratios. Chem Geol 199(3–4):281–292. https://doi.org/10.1016/S0009-2541(03)00128-1

Ibrahim RGM, Korany EA, Tempel RN, Gomaa MA (2019) Processes of water-rock interactions and their impacts upon the groundwater composition in the Assiut area, Egypt: Applications of hydrogeochemical and multivariate analysis. J Afr Earth Sc 149:72–83. https://doi.org/10.1016/j.jafrearsci.2018.07.026

Jeevananda M, Nagarajan R, Manikandan M, Senthilkumar M, Srinivasalu S, Prasanna MV (2012) Hydrochemistry and microbial contamination of groundwater from Lower Ponnaiyar Basin, Cuddalore District, Tamil Nadu. India Environ Earth Sci 67(3):867–887. https://doi.org/10.1007/s12665-012-1534-1

Kloppmann W, Bourhane A, Asfirane F (2011) Méthodologie de diagnostic de l'origine de la salinité des masses d'eau. Emploi des outils géochimiques, isotopiques et géophysiques. Rapport BRGM/RP-60026-RP, 129p.

Kumar PJS (2014) Evolution of groundwater chemistry in and around Vaniyambadi Industrial Area: differentiating the natural and anthropogenic sources of contamination. Chem Erde 74(4):641–651. https://doi.org/10.1016/j.chemer.2014.02.002

Liu Y, Jiao JJ, Liang W, Kuang X (2017). Hydrogeochemical characteristics in coastal groundwater mixing zone. Appl. Geochem. 85: 49e60. https://doi.org/10.1016/j.apgeochem.2017.09.002.

Llamas MR, Martínez-Santos P (2005) Intensive groundwater use: silent revolution and a potential source of social conflicts. J Water Resour Plan Manag 131(5):337–341. https://doi.org/10.1061/(ASCE)0733-9496(2005)131:5(337)

Loni OA, Zaidi FK, Alhumimidi MS, Alharbi OA, Hussein MT, Al DM, Yousef KA, Kassem OMK (2015) Evaluation of groundwater quality in an evaporation dominant arid environment; a case study from the Al Asyah area in Saudi Arabia. Arab J Geosci 8(8):6237–6247. https://doi.org/10.1007/s12517-014-1623-4

Moussaoui Z, Gentilucci M, Wederni K, Hidouri N, Hamedi M, Dhaoui Z (2023) Hamed Y (2023) Hydrogeochemical and Stable Isotope Data of the Groundwater of a Multi-Aquifer System in the Maknessy Basin (Mediterranean Area, Central Tunisia). Hydrology 10:32. https://doi.org/10.3390/hydrology10020032

Mukherjee A, Bhattacharya P, Savage K, Foster A, Bundschuh J (2008) Distribution of geogenic arsenic in hydrologic systems: Controls and challenges. J Contam Hydrol 99(1–4):1–7. https://doi.org/10.1016/j.jconhyd.2008.04.002

Nagaraju A, Sunil Kumar K, Thejaswi A (2014) Assessment of groundwater quality for irrigation: a case study from Bandalamottu lead mining area, Guntur District, Andhra Pradesh. South India Applied Water Science 4(4):385–396. https://doi.org/10.1007/s13201-014-0154-1

Nazzal Y, Ahmed I, Al-Arifi NSN, Ghrefat H, Zaidi FK, El-Waheidi MM, Batayneh A, Zumlot T (2014) A pragmatic approach to studying the groundwater quality suitability for domestic and agricultural usage, Saq aquifer, northwest of Saudi Arabia. Environ Monit Assess 186(8):4655–4667. https://doi.org/10.1007/s10661-014-3728-3

Ostad-Ali-Askari et al (2021) (2021) Quantity and quality modeling of groundwater to manage water resources in Isfahan-Borkhar Aquifer. Environ Dev Sustain 23:15943–15959. https://doi.org/10.1007/s10668-021-01323-1

Ostad-Ali-Askari et al. (2019) Effect of Management Strategies on Reducing Negative Impacts of Climate Change on Water Resources of the Isfahan-Borkhar Aquifer Using MODFLOW. River Research and Applications, John Wiley & Sons Ltd. 35(6):611-631. https://doi.org/10.1002/rra.3463

Parkhurst DL (1995) Advective-transport, and inverse geochemical calculations Water-Resources Investigations Report 95–4227.

Piper AM (1944) 914 Transactions, American geophysical union times as great as it should have been. And in this case. American Geophysical Union, 914–928.

Pradhan SP, Joshi P, Poudel P (2022) Long-term assessment of water quality of Kathmandu University Drinking Water Supply Centre. Nepal Sustain Water Resour Manag 8:41. https://doi.org/10.1007/s40899-022-00636-x

Rajesh R, Brindha K, Murugan R, Elango L (2012) Influence of hydrogeochemical processes on temporal changes in groundwater quality in a part of Nalgonda District, Andhra Pradesh. India Environ Earth Sci 65:1203–1213

Rajmohan N, Elango L (2004) Identification and evolution of hydrogeochemical processes in the groundwater environment in an area of the Palar and Cheyyar River Basins. Southern India Environmental Geology 46(1):47–61. https://doi.org/10.1007/s00254-004-1012-5

Rao, G.T., Rao, V.V.S.G., Sarma, V.S., Dhakate, R., Surinaidu, L., Mahesh, J., Ramesh, G., 2012. Hydrogeochemical parameters for assessment of groundwater quality in a river sub-basin. Int. J. Environ. Sci. Technol. 9, 297e310. https://doi.org/10.1007/s13762-012-0024-z.

Shahid SU, Iqbal J, Hasnain G (2014) Groundwater quality assessment and its correlation with gastroenteritis using GIS: a case

study of Rawal Town, Rawalpindi. Pakistan Environ Monitoring Assess 186(11):7525–7537. https://doi.org/10.1007/s10661-014-3945-9

Shayannejad et al. (2022) Modeling of Surface Flow and Infiltration During Surface Irrigation Advance Based on Numerical Solution of Saint–Venant Equations Using Preissmann Scheme. Pure Appl. Geophys. https://doi.org/10.1007/s00024-022-02962-9

Su YH, Feng Q, Zhu GF, Si JH, Zhang YW (2007) Identification and Evolution of Groundwater Chemistry in the Ejin Sub-Basin of the Heihe River, Northwest China. Pedosphere, 17(3), 331–342. https://doi.org/10.1016/s1002-0160(07)60040-x.

SubRamani T, RajmoHan N, ELango L (2010) Groundwater geochemistry and identification of hydrogeochemical processes in a hard rock region. Southern India. Environ. Monit. Assess 162(1–4):123–137. https://doi.org/10.1007/s10661-009-0781-4

Talebmorad et al. (2022) Hydro geo-sphere integrated hydrologic model in modeling of wide basins. Sustain Water Resour Manag 8: 118. https://doi.org/10.1007/s40899-022-00689-y

Tirumalesh K, Shivanna K, Sriraman A, Tyagi A (2010) Assessment of quality and geochemical processes occurring in groundwaters near central air conditioning plant site in Trombay, Maharashtra. India Environ Monit Assess 163:171–184

Xiao J, Jin ZD, Zhang F, Wang J (2012) Solute geochemistry and its sources of the groundwaters in the Qinghai Lake catchment, NW China. J Asian Earth Sci 52:21–30. https://doi.org/10.1016/j.jseaes.2012.02.006

Yehdego S 2003 Hydrogeology of Ilala-Aynalem Catchments with Particular Reference to the Chemical Variation and Aquifer characteristic. MSc thesis, Addis Ababa, Ethiopia. 192pp. https://doi.org/10.1007/s11356-020-08300-7.